Article

Discrimination of Kinetic Models by a Combination of Microirradiation and Fluorescence Photobleaching

Laurin Lengert,[1,*] Nicor Lengert,[1] Barbara Drossel,[1] M. Cristina Cardoso,[2] Britta Muster,[2] Danny Nowak,[2] and Alexander Rapp[2]
[1]Institute for Condensed Matter Physics and [2]Department of Biology, Technische Universität Darmstadt, Darmstadt, Germany

ABSTRACT Fluorescence recovery after photobleaching (FRAP) is an excellent tool to measure the chemical rate constants of fluorescently labeled proteins in living cells. Usually FRAP experiments are conducted with the protein concentrations being in a steady state, i.e., when the association and dissociation of the proteins are equilibrated. This is a strong limitation because situations in which rate constants change with time are of great scientific interest. In this study, we present an approach in which FRAP is used shortly after DNA damage introducing laser microirradiation, which results in the recruitment of the DNA clamp protein proliferating cell nuclear antigen (PCNA) to DNA lesions. We establish different kinetic models that are compatible with the observed PCNA recruitment data if FRAP is not used. By using FRAP at different time points during protein accumulation, we can not only exclude two out of three models, but we can also determine the rate constants with increased reliability. This study thus demonstrates the feasibility of using FRAP during protein recruitment and its application in the discrimination of possible kinetic models.

INTRODUCTION

Fluorescently labeled proteins are a major tool in cell biology as they enable the tracking of proteins in live cells by fluorescence microscopy. Methods exist that allow observing single proteins (single particle tracking, single molecule tracking), but these techniques often suffer from the low photo-stability of fluorescent proteins (1). Therefore, in many situations bulk measurements of average behavior, such as fluorescence correlation spectroscopy or fluorescence recovery after photobleaching (FRAP), are preferred over information gathered from single particles. In FRAP experiments, which are technically less complex and, hence, more widely employed (1), the labeled proteins are irreversibly photobleached in a small area of the cell by a high-powered focused laser beam (2,3). The diffusion of the surrounding nonbleached fluorescent proteins into the bleached area leads to the recovery of the fluorescence signal, recorded using a low-powered laser (4). Hence, FRAP experiments provide a bulk measurement of the average mobility of the labeled proteins in a small volume and allow one to derive their association and dissociation rate via fitting mathematical models to the data (5–7). When protein diffusion occurs on a much faster scale than association and dissociation, simple diffusion uncoupled models can be used (8).

Usually FRAP experiments are conducted with the protein concentration being in a steady state, i.e., when the association and dissociation of the labeled proteins are equilibrated (5,7–9). However, this represents a strong limitation on the applications of FRAP. Often the protein concentrations in living cells are not in a steady state, but it would still be very interesting to derive their association and dissociation rates by conducting FRAP experiments and simulations that do not rely on the steady-state condition. An example for an external trigger after which the local protein concentration in the cells is not in a steady state is laser microirradiation. Microirradiation introduces DNA lesions, such as single- and double-strand breaks, at preselected subnuclear sites in living cells (10), which results in the physiological accumulation of the repair proteins at these sites.

In this article, we focus on the recruitment of proliferating cell nuclear antigen (PCNA) to DNA following DNA damage induction by laser microirradiation. PCNA belongs to the family of processive clamps and is involved in both DNA replication and repair (11). In mammals, PCNA forms a homotrimer that is loaded as a precomplex by the replication factor C (RFC) complex, a member of the AAA+ ATPase family, in an ATP-dependent manner. Notably, also the unloading is assumed to be achieved by the same RFC complex, again dependent on ATP hydrolysis (11,12). In replication, PCNA tethers essential factors, namely DNA polymerases, to the DNA template and thus allows high processivity (13), but also translesion synthesis and template switching if DNA damage is encountered during replication. In repair, PCNA is involved in the template processing during homologous recombination (14), in the repair of interstrand cross-links and adducts, as well as in repair-linked DNA replication in long patch base excision

Submitted January 21, 2015, and accepted for publication August 11, 2015.
*Correspondence: lengert@fkp.tu-darmstadt.de
Editor: Catherine Royer

0006-3495/15/10/1551/14
http://dx.doi.org/10.1016/j.bpj.2015.08.031

and nucleotide excision repair (15,16). To achieve its multiple functions in DNA replication and repair, PCNA is seen as a molecular platform for diverse protein-protein interactions. Binding to PCNA occurs mainly at a conserved region of the monomer via the motif PCNA-interacting peptide (PIP) box (11,17). A second interaction site is recognized by the AlkB homolog 2 PCNA-interacting motif (APIM) (11,18). Although the first one is mostly related to replication interactions, the latter is mainly involved in interactions following DNA damage. Today several hundred proteins have been identified that contain either PIP or APIM motifs and still others bind to PCNA independently of both (11). The regulation of these multiple interactions is tightly controlled on several levels. First, different binding affinities of the partners result in preferential binding (e.g., p21 has a high affinity to the PIP box and can displace polymerase delta subunit p66 to halt the cell cycle (19). Second, a complex posttranslational modification pattern (PTM) is known to influence PCNA interactions. The most important PTMs are mono-, polyubiquitination, and SUMOylation, but also phosphorylation and acetylation (14,20).

The response of cells to DNA damage is a vast field of research (21). Usually, protein recruitment to the damaged site is evaluated by measuring the time dependence of the fluorescence signal in the region of interest (damage site). By fitting kinetic models to the measured data one attempts to evaluate association and dissociation rates as well as the rate with which the DNA is repaired. Unfortunately, in many cases there are different models with the same number of parameters that fit the data equally well (6,22). In such situations, additional information is of great value. Therefore, in this article we show that it is possible to conduct FRAP experiments during the time of PCNA accumulating at sites of DNA damage. To our knowledge, this type of measurement has not been done before. As a proof of concept we show that FRAP during nonsteady state is possible and leads to additional information about the protein kinetics, which can be used to discriminate between different protein recruitment scenarios.

MATERIALS AND METHODS

Cell culture and transfection

HeLa Kyoto (23) cells stably expressing mCherry-PCNA (24) were cultivated in the presence of blasticidin (2.5 μg/ml). For microirradiation experiments cells were grown on cover slide dishes.

Western blot analysis

HeLa Kyoto cells were grown to 80% confluence and harvested by trypsinization. Cell pellets of 2×10^6 cells were resuspended in 100 μl of phosphate buffered saline (PBS) + 35 μl 4× sodium dodecyl sulfate loading buffer, boiled, and the amount indicated was loaded on a 12% sodium dodecyl sulfate page. After electrophoresis and blotting the membrane was blocked in 1% Roti-Block for 30 min. PCNA was detected by rat anti-PCNA (clone 16D10 (25)), diluted 1:1000 in PBS including 1% Roti-Block, and then diluted 1:2000 by anti-rat-IgG-Cy5 (Jackson Immuno Research, Suffolk, UK). Blots were analyzed using the STORM imager and bands were quantified with Image Quant 5.2 (GE Healthcare, Freiburg, Germany).

Flow cytometry and high-content imaging

For flow cytometry, exponentially growing cells were trypsinized and dispensed as single-cell suspension. Cells were fixed in 70% ice-cold methanol for 30 min at 4°C. Flow analysis was carried out using a S3 flow cytometer (Biorad) with a 561 nm laser for excitation and a 560 nm beam splitter and a 585/25 nm emission filter. Cells were gated for singlets and the fluorescence was recorded for >10,000 cells. For high-content imaging, the cells were seeded on cover slips and fixed in 3.7% formaldehyde in PBS for 20 min at room temperature. Cells were mounted after DAPI staining in moviol (Sigma Aldrich, Taufkirchen, Germany). Image acquisition was performed using a 20× LD 0.45 NA objective in an Operetta (Perkin Elmer, Rodgau, Germany) high-content screening system. mCherry was imaged using a 560 to 580 nm excitation filter together with an emission filter 590 to 640 nm. Image analysis was performed using the Harmony software (Perkin Elmer) with the following pipeline: 1) find nuclei, method M, guide size 15 μm, splitting coefficient 0.2, and common threshold 0.4; 2) exclude out-of-focus and touching nuclei by population filtering: Haralick contrast 4px <0.8, nucleus area >100 μm^2 and <300 μm^2, and roundness >0.83; and 3) measure the mean and total intensity of mCherry in the nucleus.

Laser microirradiation and FRAP

Imaging and microirradiation experiments were performed using an UltraVIEW VoX spinning disc confocal system (Perkin Elmer) in a closed live-cell microscopy chamber (ACU, Perkin Elmer) at 37°C with 5% CO_2 and 60% humidity, mounted on a Nikon TI microscope (Nikon, Düsseldorf, Germany).

Images were taken with a CFI Apochromat 60×/1.49 NA oil immersion objective. For imaging of mCherry-PCNA, we used 561 nm laser excitation and a 612 ± 70 nm (full width at half maximum) emission filter. For imaging, the 561 nm laser was set to 10%. It is important to note that with every image taken a small amount of the proteins were bleached.

For microirradiation, only cells not in S phase were used. In those cells a preselected spot (1 μm diameter) within the nucleus was microirradiated for 1.2 s with a 405 nm laser set to 100%, resulting in 0.99 mJoule. This laser has been reported to cause single- and double-strand breaks as well as oxidative base damage (26).

Photobleaching of mCherry-PCNA at previously microirradiated sites was performed using a circular region of interest (1 μm diameter) for 1 s with a 561 nm laser set to 100% resulting in 6.7 mJoule. Energy output was measured with a laser power meter (Ophir Optronics, Irvine, CA) directly after the objective with beam park settings. Before and after microirradiation and photobleaching, confocal image series of one mid-nucleus z section were recorded as 16-bit images in 2 s intervals.

It is important to note that the 561 nm laser does not cause DNA damage to which PCNA is recruited (see Fig. S1 in the Supporting Material).

Image analysis

All analysis steps for the confocal microscopy images were performed using imageJ (27). For data analysis we marked by hand the total nuclear area (*green circle* in Fig. 1) from which we derived the nucleus fluorescence signal (NFS) by integrating the intensity over all pixels within this area (the size of the area is denoted by NFS_{Area}). Additionally, we marked a small region that was either outside the nucleus or outside the cell (*blue*

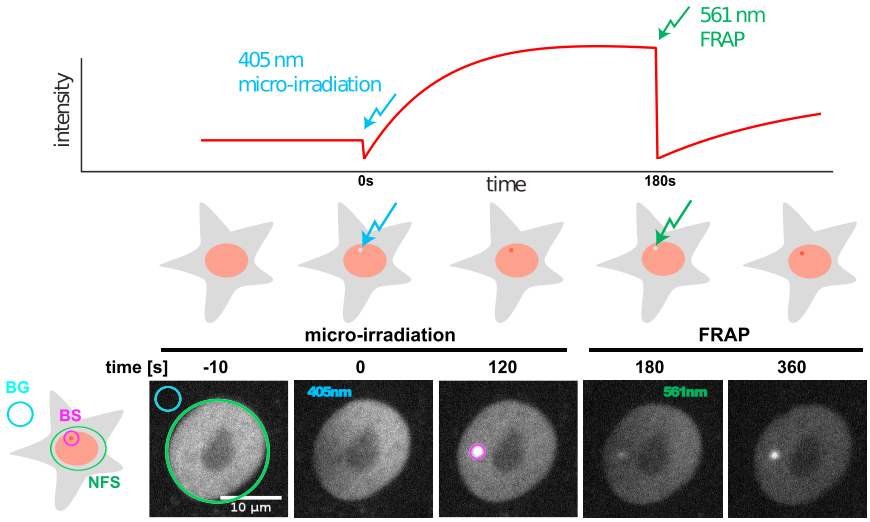

FIGURE 1 Schematic procedure and actual images of an experiment including FRAP. For data analysis we marked by hand the nucleus area (*green circle*) from which we derived the nucleus fluorescence signal (NFS). Additionally, we marked a small region that was either outside the nucleus or outside the cell (*blue circle*) to measure the background signal (BGS) as well as the microirradiated spot (*purple circle*) to measure the bleachspot signal (BS). To see this figure in color, go online.

circle in Fig. 1, the size of the area is denoted by BGS_{Area}) to measure the background signal (BGS). Last, we marked the microirradiated spot (*purple circle* in Fig. 1, the size of the area is denoted by BS_{Area}) to measure the bleachspot signal (BS).

This data analysis aims at deriving the concentration of recruited PCNA within the bleachspot. Because the signal in the bleachspot is caused by both the freely diffusing proteins and the proteins bound to the DNA, we need a method to estimate the fraction of the signal attributed to the freely diffusing proteins within the bleachspot. As we show in the Supporting Material, the concentration of freely diffusing proteins does not significantly change over time (if corrected for bleaching). Hence, we measure the mean intensity value of the bleachspot signal before the irradiation (denoted by $\overline{BS_0}$), which we corrected for the background signal, and use it as an approximation for the signal caused by the free proteins within the bleachspot for every time point. Additionally, we confirmed that the FRAP measurement is not influenced by diffusion, by following Sprague et al. (28). We compared FRAP curves of both freely diffusing and microirradiation accumulated PCNA with ROIs of different sizes, and we found no significant difference between the different ROIs, as shown in Fig. S1.

We need to consider that each time we use a laser (for microirradiation, photobleaching, or imaging), this inevitably leads to the bleaching of some proteins. Hence, the fluorescence signal will decrease with each image taken, even if the proteins did not exchange in and out at all. To take this bleaching effect into account, we evaluated the NFS for each image, NFS(t), and compared it with the mean value before microirradiation, $\overline{NFS_0}$. Both of these values were corrected for background signal. With this, the bleaching factor $BF(t) = (NFS(t) - BGS(t)(NFS_{Area}/BGS_{Area}))/(\overline{NFS_0} - BGS_0(NFS_{Area}/BGS_{Area}))$ quantifies the bleaching effect, and the fluorescence signal of bound proteins (FSBP) is given by the following:

$$FSBP(t) = \frac{1}{BF(t)}\left(BS(t) - BGS(t)\frac{BS_{Area}}{BGS_{Area}}\right) - \left(\overline{BS_0} - BGS_0\frac{BS_{Area}}{BGS_{Area}}\right), \quad (1)$$

where $\overline{BS_0} - BGS_0(BS_{Area}/BGS_{Area})$ is the approximated signal caused by the freely diffusing proteins within the bleachspot (corrected for background).

So far, we have dealt with the fluorescence signal of the proteins, but not with the actual concentration. To derive the concentration, a factor is needed, which converts the fluorescence signal into protein amounts (denoted by v), from which we derive the concentration by dividing through the observed volume of the bleachspot. We estimate this factor from known data. A precise knowledge of this factor is not necessary because it does not affect the results for the fitted rate constants. Changing this factor affects all terms in our equations equally, because they are proportional to the concentration of the labeled protein. From measuring the NFS in each cell before microirradiation, we know that the amount of fluorescently labeled proteins is approximately the same in each cell besides the variation between G1 and G2 phase. Additionally, we assessed the variation in the level of the recombinant protein by flow cytometry and high-content imaging. The mCherry-PCNA signal in both methods showed a variation within the twofold regulation found for the endogenous one (29). To measure the ratio between endogenous PCNA and the stably transfected mCherry-PCNA, we performed quantitative Western blotting with cell lysates of the stable HeLA-Kyoto mCherry-PCNA cell line (Fig. S2). From these data we established a ratio of 8.1 ± 2.7 between the unlabeled and labeled PCNA. The total amount of endogenous PCNA did not change in the stable cell line.

According to Morris and Mathews (29), the number of PCNA molecules per HeLa cell is 3.6×10^5 during G1 phase and 11.4×10^5 during G2 phase. From the cells used in our experiments, 18.5% were in G2 (distinguished by their roughly 1.3-fold larger area) and 81.5% of the cells were in G1. Hence, according to the findings of Morris and Mathews the average number of PCNA molecules in our cells is supposed to be $(18.5 \times 11.4 + 81.5 \times 3.6)10^3 \approx 5 \times 10^5$. Additionally, it is important to note that according to Morris and Mathews (29) the fraction of PCNA bound to chromatin is negligible in cells that are not in S phase. Therefore, $5 \times 10^5/8.1$ is the average amount of tagged proteins in each cell.

Taking the mean value of the NFS before microirradiation ($\overline{NFS_0}$) from all cells and averaging over the cells (giving $\overline{\overline{NFS_0}}$), the factor that converts the fluorescence signal into protein amount can be written as the following:

$$v = \frac{500000/8.1}{\overline{\overline{NFS_0}}}. \quad (2)$$

Besides this factor, the observed volume of the bleachspot needs to be known to compute the protein concentration. For the theoretical models, it is important that the concentration of bound PCNA is computed based on the same volume. Hence, we used the largest bleachspot area from all cells of an experiment (denoted by $BS_{Area,Max}$ with a size of ~4 μm^2) each time we computed the concentration of bound PCNA. To obtain the volume, this area is multiplied by the depth in z direction, which is determined by the width $w_z = 1.1$ μm of the point spread function of the imaging system, which is shown in Fig. S3, *B* and *C*. With this, the concentration of

bound (and fluorescently labeled) PCNA proteins within the bleachspot can be calculated using the following formula:

$$\begin{aligned}\mathrm{PCNA_{bound}(t)} &= \frac{v}{\mathrm{BS_{Area,Max}}w_z}\mathrm{FSBP(t)}\\ &= \frac{v}{\mathrm{BS_{Area,Max}}w_z}\left(\frac{1}{\mathrm{BF(t)}}\left(\mathrm{BS(t)}-\mathrm{BGS(t)}\frac{\mathrm{BS_{Area}}}{\mathrm{BGS_{Area}}}\right)-\left(\overline{\mathrm{BS}}_0-\mathrm{BGS}_0\frac{\mathrm{BS_{Area}}}{\mathrm{BGS_{Area}}}\right)\right).\end{aligned} \tag{3}$$

Theoretical models

To understand which are the most important processes that lead to the characteristic recruitment curves of PCNA in our experiments, we developed several theoretical models. These models are as simple as possible mainly for two reasons. First, with increasing complexity (i.e., the number of chemical species and reactions included into the model) any model will be able to fit almost every experimental data well. This makes it impossible to discriminate between different models based on their ability to reproduce the data.

Second, with more complex models it becomes impossible to see which are the most important ingredients of the model needed to reproduce the data. For example, an interesting feature of our data is the overshoot that can be seen in the PCNA recruitment curves (Fig. 2: the curves peak early on and then decrease till they reach a plateau).

A model for FRAP recovery during nonsteady state has already been proposed by Lele and Ingber (30) that leads to the conclusion that the overshoot observed in the experimental curves can be caused by a disassembly of the structural scaffold. But in that model the number of available scaffold binding sites decays exponentially, and thus it would not be able to reproduce both features of the experimental data, the steep slope as well as the long stretched plateau. Also, the disassembly is implemented phenomenologically without specifying the underlying mechanism.

There are other possible reasons causing an overshoot. First, similar to the model mentioned (30), instead of a general disassembly, the reduction of available binding sites is attributable to the repair of different kinds of DNA damage at different rates. Those damages, induced by the laser microirradiation, could be single strand break, double strand break (DSB), or oxidative base damages (31) resulting in a different (mixed) PCNA recruitment and release kinetics (32,33). Second, the recruitment of PCNA could be influenced by another protein, which changes its dissociation rate, e.g., by posttranslational modifications such as ubiquitination (34). Third, another reason for the overshoot might be that the endogenous PCNA proteins (which are not fluorescently labeled and therefore invisible in our experiments) have different association and dissociation rates compared with the tagged PCNA proteins. We will make a minimal model for all three of these scenarios.

It is important to note that in our modeling approach we fit all experimental data sets at once using the same parameters for every experiment if possible. For example, we conducted 13 experiments that include a FRAP bleach. When fitting the resulting curves from these experiments we use the same chemical rate constants for all 13 fits. This method considerably decreases the number of free parameters and thereby reduces the freedom of the fit algorithm and hence the uncertainty of the parameters.

All models we discuss consist of two or three chemical species. At least one of them is a substrate (S), such as a single-strand break in the DNA, a double-strand break, or an oxidative base damage, which all can be induced by the 405 nm laser (26). The second species is a protein (P) binding to the substrate. We assume that the relations between these species are composed of elementary reactions such as the following:

$$S + P \xrightarrow{k_{S+P\to SP}} SP, \tag{R1}$$

and

$$SP \xrightarrow{k_{SP\to S+P}} S + P. \tag{R2}$$

Here, P denotes a PCNA protein, S represents damage containing DNA, SP is the complex (e.g., PCNA bound to the DNA), and $k_{S+P\to SP}$ and $k_{SP\to S+P}$ denote the forward and backward reaction rate constant. PCNA is a trimer and we assume that either it is recruited to the DNA as a preformed trimer or

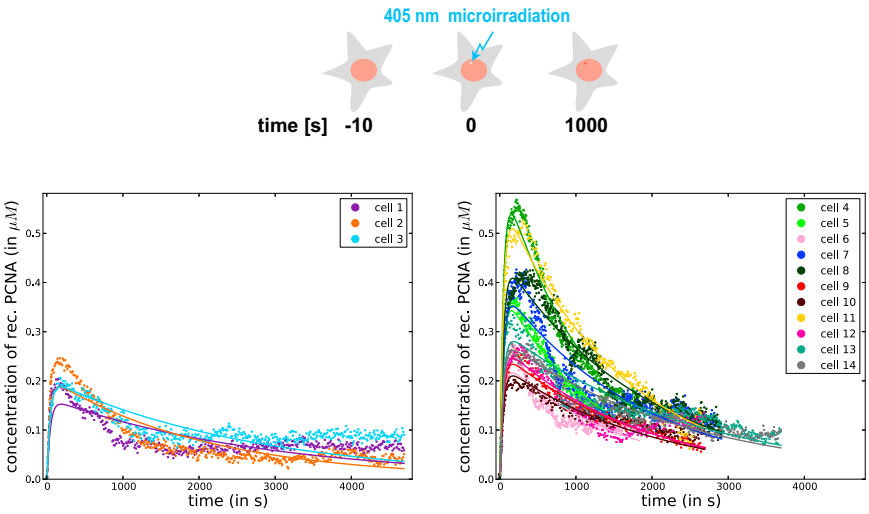

FIGURE 2 Protein recruitment data of the microirradiation experiments for 14 cells. The experimental data is shown as dots and the fits are shown as lines of the same color. Experimental setup according to scheme on top. The fit uses the most simple model out of those with the ability of producing an overshoot (basic model plus one reaction for DNA repair). The model includes only the binding of PCNA to damaged sites and repair of the DNA followed by dissociation of PCNA. In this fit we did not use cross-validation, hence all 14 curves are fitted simultaneously with the chemical rates being free parameters. Still, the model is unable to fit the plateau following the overshoot (see cell 1 to 3 at $t > 1800$ s). $\chi^2 \approx 1.9 \times 10^5$ and the number of fitted data points was 6320. To see this figure in color, go online.

that the trimerization happens on a faster timescale compared with the overall recruitment and release of PCNA; and therefore in our model only the trimer is included (denoted by P). Knowing that PCNA recruitment happens on a slower timescale compared with diffusion (see section about control experiments in the Supporting Material and Fig. S1) and using the law of mass action these chemical reactions can be translated into the following set of differential equations for the concentrations of the chemical species:

$$\frac{d[SP]}{dt} = -\frac{d[P]}{dt} = -\frac{d[S]}{dt} = k_{S+P\to SP}[P][S] - k_{SP\to S+P}[SP]. \tag{4}$$

These equations represent our basic model. It is too simple to reproduce an overshoot similar to the one that can be seen in our experimental data (see Fig. S3: the solution is a monotonously increasing, monoexponential function). Hence, in the different models we present later starting from this basic model we will add more chemical reactions and/or species, which are needed to reproduce such an overshoot. The considered additions to the basic model are the following:

1) The dissociation of PCNA after its task at the DNA damage site is completed. After this point, the damage is treated as repaired in our model, even though there might be subsequent PCNA independent steps. In this case the following chemical reaction is added to the following basic model:

$$SP \xrightarrow{k_{Repair}} P. \tag{R3}$$

2) The presence of a second kind of DNA damage (e.g., a double-strand break denoted by D) is shown in the following:

$$D + P \xrightarrow{k_{D+P\to DP}} DP, \tag{R4}$$

$$DP \xrightarrow{k_{DP\to D+P}} D + P. \tag{R5}$$

3) A second protein influences the dissociation rate constant of PCNA but is not influenced by PCNA in turn. To keep the model as simple as possible the dissociation of the second protein is not included and there is only one kind of DNA damage included. Even if in the experiments several kinds of DNA damage lead to the recruitment of PCNA, this model can be a valid description under the assumption that the chemical rates of PCNA do not depend on the type of damage. This second protein is denoted by A and the DNA damage to which both proteins, PCNA and the second protein, have been recruited is denoted by SPA in the following:

$$S + A \xrightarrow{k_{S+A\to SA}} SA, \tag{R6}$$

$$SP + A \xrightarrow{k_{SP+A\to SPA}} SPA, \tag{R7}$$

$$SA + P \xrightarrow{k_{SA+P\to SPA}} SPA, \tag{R8}$$

$$SPA \xrightarrow{k_{SPA\to SA+P}} SA + P. \tag{R9}$$

4) In the last model we assume that the endogenous PCNA proteins have different association and dissociation rates compared with the tagged PCNA proteins. According to previous findings, the binding of tagged and untagged endogenous proteins is of equal strength (24). Nevertheless, we included this model to test whether the new approach, to our knowledge, presented in this article supports these previous insights. The endogenous PCNA proteins are denoted by E:

$$S + E \xrightarrow{k_{S+E\to SE}} SE, \tag{R10}$$

$$SE \xrightarrow{k_{SE\to S+E}} S + E. \tag{R11}$$

We translated these reactions into rate equations just as was done with Eq. 4. Such deterministic modeling is valid if the concentrations of the chemical species in the modeled volume are so high that the stochastic nature of the underlying processes is negligible. Even if this is not the case, the deterministic description is still useful as an approximation.

To solve these differential equations we used the Runge-Kutta Cash-Karp method as implemented in the GNU Scientific Library. Because the algorithm to solve the differential equations was very slow when using very low or high values for the concentrations and rate constants, they were limited to be in the range $[e^{-25}, e^{25}]$. Because the use of penalty functions for restricting parameter values often causes problems, we achieved the limitation by performing the fitting algorithm with new parameters κ_{new}. Here, κ_{new} denotes any parameter (rate constant or protein concentration). The new parameters are derived from the old parameters (κ) by using the formula $\kappa_{new} = e^{25\cdot sin(\kappa)}$.

As shown in the control experiments (see Supporting Material), the concentration of freely diffusing proteins is approximately constant. Hence, we set in all models $[P](t) = P_0$.

To find the best fit given a specific model and data, we used an algorithm based on the covariance matrix adaptation evolution strategy (35). The initial value of the freely diffusing protein concentration is set to $P_0 = \overline{\mathrm{BS}}_0$ (mean value of the bleachspot signal before microirradiation). Additionally, we limit the fit algorithm to use values in the following range:

$$0.8 \times \overline{\mathrm{BS}}_0 \le P_0 \le 1.2 \times \overline{\mathrm{BS}}_0. \tag{5}$$

Hence, we allowed P_0 to deviate from $\overline{\mathrm{BS}}_0$ by 20%. This value is roughly estimated from the control experiments shown in Fig. S4, in which the concentration of PCNA in a nonbleached region showed only a small variation in time (if excluding the values right after microirradiation and FRAP bleach). The results we present later are not sensitive to the exact value of this deviation. Hence, this rough estimation is sufficient. We use the same values for the rate constants in all cells (all data sets are fitted simultaneously), which helps reducing the parameter space.

Because we do not have direct data for the DNA damage or for other protein concentrations besides PCNA, the fit algorithm may choose any positive value that fits the data well. Unless declared otherwise, the initial value for S_0 is drawn randomly between 10^2 and 10^{-4} (and then, as described before, limited to the range $[e^{-25}, e^{25}]$). The initial values for the rate constants are drawn analogously. The reasoning is that initial values outside of this scope lead to theoretical curves that have a large deviation to the experimental curves. Hence, those initial values do not seem feasible and additionally they often lead to the fit algorithm failing at finding a good fit (it converges to a set of parameters that obviously is not the best solution).

Curve fitting and cross-validation

To measure the goodness of the fit we used χ^2 in the following:

$$\chi^2 = \sum_T \frac{(\mathrm{PCNA}_{\mathrm{bound}}[T] - \mathrm{PCNA}_{\mathrm{theo}}[T])^2}{\sigma^2[T]}. \tag{6}$$

The sum is calculated over all data points, $\mathrm{PCNA}_{\mathrm{bound}}[T]$ is the Tth experimental value of bound PCNA and $\mathrm{PCNA}_{\mathrm{theo}}[T]$ is the Tth theoretical value of bound PCNA (in the case of the two kinds of DNA damage model: $\mathrm{PCNA}_{\mathrm{theo}}[T] = SP[T] + DP[T]$). $\sigma^2(T)$ is the moving variance of the

experimental data. To calculate this moving variance, we calculated the moving average first. Because for each time point in each curve we had only one value, we calculated the moving average by using the two data points before and the two data points after that value in the following:

$$\begin{aligned}\overline{\mathrm{PCNA}_{\mathrm{bound}}}[T] &= \left(\sum_{i=T-2}^{i=T+2}\mathrm{PCNA}_{\mathrm{bound}}[i]\right)\Big/5\\ &= (\mathrm{PCNA}_{\mathrm{bound}}[T-2]+\mathrm{PCNA}_{\mathrm{bound}}[T-1]+\mathrm{PCNA}_{\mathrm{bound}}[T]+\mathrm{PCNA}_{\mathrm{bound}}[T+1]+\mathrm{PCNA}_{\mathrm{bound}}[T+2])/5.\end{aligned} \tag{7}$$

With this moving average we calculated the moving variance in the following in a similar way:

$$\sigma^2[T] = \left(\sum_{i=T-2}^{i=T+2}\left(\mathrm{PCNA}_{\mathrm{bound}}[i]-\overline{\mathrm{PCNA}_{\mathrm{bound}}}[T]\right)^2\right)\Big/5. \tag{8}$$

If the above calculation was not applicable (e.g., for the data points right before and after the FRAP bleach), we used the variance of the data points before microirradiation.

Small values of χ^2 indicate a good fit, whereas large values indicate a bad fit. Hence, the fit algorithm was set to minimize the value of χ^2.

To further test whether or not a model is able to fit the data well, we used a cross-validation approach. From the 13 curves in the FRAP experiments (14 curves in the experiments without FRAP) we used 10 curves as the training data set. Hence, the fit algorithm described above was set to minimize χ^2 given the 10 experimental curves from the training data set and a specific model, where the kinetic rates and the initial concentrations (P_0 limited by Eq. 5) were used as fitting parameters. Next we used the remaining curves as the validation set: the chemical rates of the model were set to the values derived from the training set and the fit algorithm minimized χ^2 from the validation curves. In the validation fits for each curve, there were two free parameters S_0 and P_0, the latter limited by Eq. 5. In the two kinds of DNA damage model the initial value of DSBs, D_0, is an additional free parameter for each curve, whereas in the influenced dissociation rate model for each curve the additional free parameter is the concentration of the influencing protein, A_0.

For a specific model we used this cross-validation approach four times so that each curve was part of the validation set once. Because the total number of curves was 13 (14 curves in the experiments without FRAP), the first validation set was composed of four curves, the second validation set consisted of three curves (four curves in the experiments without FRAP) and the last two validation sets consisted of three curves. To determine how well a model fitted the data, we calculated the sum of χ^2 for all four validation sets and compared the result with those from the other models. Because some of the models proposed in the last section could lead to a FRAP recovery that is dependent on the FRAP time point chosen, a late time point was used for one of the data sets to increase the information about the interaction at the DNA damage site and thus the possibility to discriminate between different models.

RESULTS

In this section we show the data from protein recruitment measurements after microirradiation with and without FRAP, and we fit the curves to the theoretical models. First, we show the recruitment curves of the microirradiation experiments to motivate the microirradiation-FRAP experiments and the choice of models.

Modeling of microirradiation experiments

The results of 14 single-cell microirradiation experiments (without FRAP) can be seen in Fig. 2. The figure shows the concentration of recruited PCNA proteins (*dotted curves*) within the bleachspot derived from the experiments as explained in the methods section (Eq. 3). At the beginning of each experiment the DNA was damaged, which led to the recruitment of the tagged PCNA. At around 5 min the recruitment curves reach a maximum after which they decline till they reach a plateau at around 30 min. We refer to this feature of the recruitment curves as overshoot. We employed a low level of microirradiation damage to measure repair kinetics. Under conditions of higher damage levels or pure UVC exposure, these kinetics are more difficult to measure (36).

Before the plateau is reached, the association and dissociation rate of PCNA are obviously not equilibrated and classical FRAP experiments cannot be performed. To fit these data we used our most simple model besides the basic model. This model only includes two chemical species, the PCNA protein and sites of DNA damage, as well as two chemical reactions: the binding of PCNA to the damaged DNA (Eq. R1) and the repair of the damage and the subsequent dissociation of PCNA (Eq. R3). In this model the two latter steps (repair and dissociation) happen simultaneously to keep the model as simple as possible. This assumption is good if the rate of repair is considerably slower than the rate of subsequent dissociation (which not necessarily equals the rate of dissociation from a site of unrepaired DNA damage). Describing the whole repair process by a model, which includes the recruitment of only one protein is a good approximation if the recruitment of PCNA is the rate-limiting step in the modeled processes.

Fig. 2 shows the best fit of this model using the χ^2 method explained in the theoretical models section. In this fit we did not use cross-validation, hence all 14 curves are fitted simultaneously with the chemical rates being free parameters. We did this to test whether or not this model is able to fit the data at all.

This simple model is able to reproduce the overshoot, but it fails at reproducing the plateau after ~1800 s (see cell 1 to

3 in Fig. 2) because for sufficiently long times all damage is repaired in this model, and the concentration of recruited protein must therefore return to zero.

In the next subsections, we will discuss different models that are able to reproduce the overshoot followed by a plateau.

Two kinds of DNA damage model

One possible explanation for an overshoot followed by a plateau is the presence of two kinds of DNA damages (e.g., single-strand breaks and double-strand breaks), which are repaired at different rates. In such a scenario the overshoot would be caused by the quick repair of the first kind of DNA damage whereas the reason for the plateau would be the second kind of DNA damage being repaired on a timescale longer than the period of the experiment.

This model consists of the chemical reactions from the basic model (Eqs. R1 and R2) to which the chemical reactions Eqs. R3, R4, and R5 were added. To keep the model as simple as possible the association and dissociation rate constants of PCNA do not depend on the kind of DNA damage ($k_{S+P\to SP} = k_{D+P\to DP}$ and $k_{SP\to S+P} = k_{DP\to D+P}$). The only difference between both kinds of damage is that the first damage can be repaired during the observed time span whereas the second cannot.

Fig. 3 *A* shows the validation fits of this model to the microirradiation. The parameter values are shown in Table 1. The curves from cells 5 to 14 were used as the training set (see Fig. S5) to determine the chemical rates, whereas the curves from cells 1 to 4 were used as the validation set. Both, the overshoot and the plateau, can be reproduced. Interestingly, in this validation fit and also in the fits of the other three validation sets the dissociation rate constant (for this fit: $k_{SP\to S+P} \approx 1.7 \times 10^{-11}$, see Table 1 for the other validation sets) is eight orders below the dissociation rate constants of the fits in the experiments with FRAP (for the four validation sets of the microirradiation-FRAP data $k_{SP\to S+P}$ is in between 4.3×10^{-3} and 6.2×10^{-3}, see lower part of Table 1), which we will show in a following section.

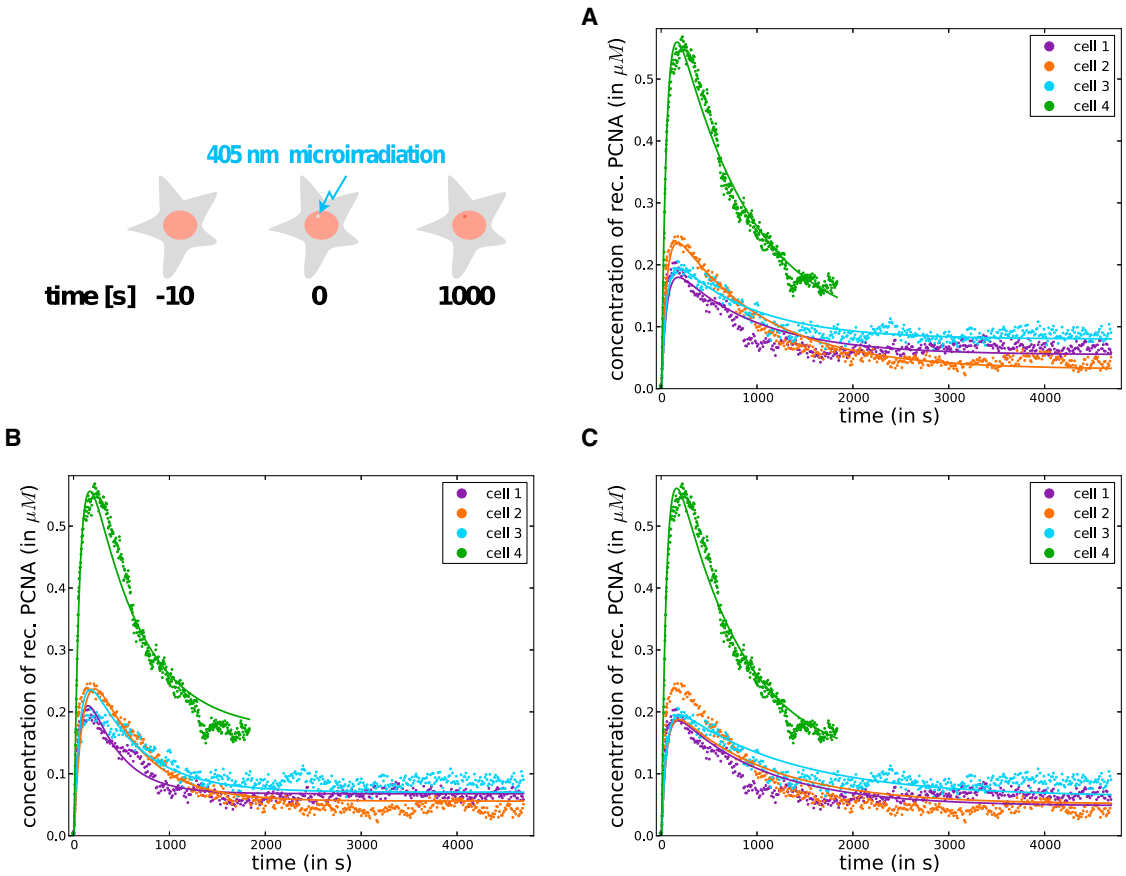

FIGURE 3 (*A*) Validation fits of the two kinds of DNA damage model to the microirradiation data. For this model, $\chi^2 \approx 2.9 \times 10^4$ and the parameter values are shown in the first row of Table 1. (*B*) Validation fits of the model in which the dissociation rate of PCNA is influenced by a hypothetical protein denoted by *A*. For this model, $\chi^2 \approx 4.1 \times 10^4$ and the parameter values are shown in the first row of Table 2. (*C*) Validation fits of the different rates for endogenous proteins model. For this model, $\chi^2 \approx 5 \times 10^4$ and the parameter values are shown in the first row of Table 3. For all three fits, the curves from cells 5 to 14 were used as the training set (see Fig. S5) and those from cells 1 to 4 as the validation set. The experimental data is shown as dots and the fits are shown as lines of the same color. Experimental setup according to scheme on top. To see this figure in color, go online.

TABLE 1 Parameter values for the two kinds of DNA damage model

Composition of Validation Set	$k_{S+P\rightarrow SP}$ ($\mu M^{-1}s^{-1}$)	$k_{SP\rightarrow S+P}$ (s^{-1})	k_{repair} (s^{-1})	χ^2	No. of Data Points
Microirradiation					
Cells 1–4	3.4×10^{-4}	1.7×10^{-11}	1.9×10^{-2}	2.9×10^{4}	1980
Cells 5–8	4.1×10^{-4}	1.5×10^{-11}	1.7×10^{-2}	3.7×10^{4}	2340
Cells 9–11	4.6×10^{-4}	1.4×10^{-11}	1.7×10^{-2}	2.7×10^{4}	900
Cells 12–14	4.2×10^{-4}	1.5×10^{-11}	1.6×10^{-2}	2.7×10^{4}	1100
Sum				1.2×10^{5}	6320
Microirradiation-FRAP					
Cells 1–4	3.5×10^{-3}	4.3×10^{-3}	1.3×10^{-3}	1.2×10^{5}	7000
Cells 5–7	2.9×10^{-3}	5.8×10^{-3}	1.6×10^{-3}	5.7×10^{4}	2950
Cells 8–10	3.4×10^{-3}	6.2×10^{-3}	1.5×10^{-3}	6.7×10^{4}	1800
Cells 11–13	2.8×10^{-3}	5.2×10^{-3}	2.3×10^{-3}	1.2×10^{5}	4650
Sum				3.5×10^{5}	16,400

The composition of the validation set is given in the column on the left.

Influenced-dissociation-rate model

Another explanation for an overshoot concentration profile followed by a plateau is that the dissociation rate of PCNA is influenced by another protein, which is not seen in the experiment. Support for such a model comes also from known posttranslational modifications of PCNA, such as acetylation (37), which is formed by another proteins. Hence, this model consists of PCNA, one kind of DNA damage and a second protein denoted by A. Both proteins, PCNA and A, can bind to the damaged DNA. This model consists of the chemical reactions from the basic model (Eqs. R1 and R2) to which the chemical reactions R6 to R9 are added. For reasons of simplification, protein A does not dissociate from the DNA whereas PCNA does. Additionally, the dissociation rate of PCNA depends on whether or not protein A is bound to the same damaged site or not: if PCNA is solely bound to the DNA (in this case the constant $k_{SP\rightarrow S+P}$ is used) the dissociation rate is lower than when it is bound in the presence of protein A (in this case the constant $k_{SPA\rightarrow SA+P}$ is used). In this model we assume that the full repair of damaged DNA happens on a slower timescale compared with the duration of the experiment, so that no chemical reaction describing the full repair of the DNA is needed.

Fig. 3 *B* shows the cross-validation fit of this model. Again, the curves from cells 1 to 4 were used as the validation set. This model is able to reproduce an overshoot followed by a plateau similar to the one in the experimental data. However, the fit of the plateau (curves 1 to 3 at $t >$ 1800 s) is worse compared with the two kinds of DNA damage model. Hence, the χ^2 of this validation set is larger compared with the same validation set in the two kinds of DNA damage model ($\chi^2 \approx 4.1 \times 10^4$ vs. $\chi^2 \approx 2.9 \times 10^4$). Nevertheless, the sum of χ^2 over all four validation sets is the same for both, the influenced dissociation rate model and the two kinds of DNA damage model ($\sum \chi^2 \approx 1.2 \times 10^5$ in both cases). Hence, from the fits of the microirradiation data it is not possible to decide which model fits the data better. Interestingly, in all the validation fits of this model the dissociation rate constant of PCNA in the absence of A is similarly low as it was in the two kinds of DNA damage model (in the microirradiation part of Table 2 $k_{SP\rightarrow S+P}$ is in between 2.4×10^{-11} and 2.5×10^{-10}). Again, this is many orders below $k_{SP\rightarrow S+P}$ in the validation fits of this model and the microirradiation-FRAP data (in the microirradiation-FRAP part of Table 2 $k_{SP\rightarrow S+P}$ is in between 5.1×10^{-3} and 6.1×10^{-3}).

Model with different association and dissociation rates for endogenous proteins

In this model we assumed that the endogenous PCNA proteins (which we do not see in our experiments) have different association and dissociation rate constants compared with the tagged proteins. The model includes again the basic reactions (R1) and (R2) to which we added the reactions (R10) and (R11), which describe the association and dissociation of the endogenous proteins. The association rate constant of the endogenous proteins is denoted by $k_{S+E\rightarrow SE}$ and the dissociation rate constant by $k_{SE\rightarrow S+E}$. As mentioned in the methods section, we know that the ratio between tagged and untagged proteins is 1:8.1. Hence, in the fits we related the concentration of freely diffusing endogenous proteins to the one of tagged proteins: $E_0 = 8.1 \times P_0$.

It is important to note that in this model the degrees of freedom are considerably fewer compared with the previous models, because there is only one free parameter per curve that can be altered freely by the fit algorithm (the concentration of DNA damages S_0). Additionally, for each curve the algorithm may adapt the value of P_0, but this is limited by Eq. 5 (the deviation between P_0 and the experimentally derived $\overline{\mathrm{BS}_0}$ is not allowed to exceed 20%). Hence, for the four curves from the validation set for this model there is a total number of four free parameters (i.e., not limited). Whereas for the two previous models there were eight free parameters for the same

TABLE 2 Parameter values for the influenced-dissociation-rate model

Composition of Validation Set	$k_{S+P\rightarrow SP}$ ($\mu M^{-1}s^{-1}$)	$k_{S+A\rightarrow SA}$ ($\mu M^{-1}s^{-1}$)	$k_{SP\rightarrow S+P}$ (s^{-1})	$k_{SPA\rightarrow SA+P}$ (s^{-1})	χ^2	No. of Data Points
Microirradiation						
Cells 1–4	3.9×10^{-3}	0.9×10^{-4}	4.5×10^{-11}	5×10^{-2}	4.1×10^{4}	1980
Cells 5–8	4.2×10^{-3}	2.1×10^{-5}	2.4×10^{-11}	6.2×10^{-2}	2.9×10^{4}	2340
Cells 9–11	4.1×10^{-3}	6.7×10^{-5}	2.5×10^{-10}	5.4×10^{-2}	1.6×10^{4}	900
Cells 12–14	3.4×10^{-3}	1.2×10^{-4}	1.8×10^{-10}	5.3×10^{-2}	3.2×10^{4}	1100
Sum					1.2×10^{5}	6320
Microirradiation-FRAP						
Cells 1–4	3.4×10^{-3}	4.9×10^{-9}	5.1×10^{-3}	3.6	2×10^{5}	7000
Cells 5–7	3.5×10^{-3}	1.2×10^{-9}	5.7×10^{-3}	0.14	5×10^{4}	2950
Cells 8–10	3.9×10^{-3}	1.4×10^{-9}	6.1×10^{-3}	0.16	7×10^{4}	1800
Cells 11–13	3.1×10^{-3}	2.8×10^{-9}	5.4×10^{-3}	5.1×10^{-2}	2.3×10^{5}	4650
Sum					5.5×10^{5}	16,400

The composition of the validation set is given in the column on the left.

validation set (in the two kinds of damage model there was the additional free parameter D_0 for each curve and in the influenced dissociation rate model A_0 was an additional free parameter for each curve).

Fig. 3 *C* shows the cross-validation fit of this model with the validation set being composed of the curves of cells 1 to 4. Again, the model is able to reproduce the overshoot and the subsequent plateau, although the validation fit to the curve of cell 2 looks worse compared with the previous models. The sum of χ^2 over all four validation sets is larger than those of the two previous models ($\sum \chi^2 \approx 1.6 \times 10^5$ as compared with $\sum \chi^2 \approx 1.2 \times 10^5$ in the two kinds of DNA damage model and the influenced dissociation rate model). Still, in comparison with the other models the sum of χ^2 is not large enough to exclude this model, especially not if considering that in the validation fits of this model the number of degrees of freedom is half that of the other two models. However, previous cell biological studies suggest that there is no difference in the biochemical properties of endogenous and recombinant protein (24,38).

Because all three models (second kind of DNA damage, influenced dissociation rate, different rates for endogenous proteins) fit the data similarly well, it is not possible to tell which of these three effects is responsible for the overshoot.

Modeling of combined microirradiation-FRAP experiments

In this section we use the microirradiation-FRAP approach to fit the previously described three models to the experimental data. In contrast to the previous section, where the fittings were not significantly different, we demonstrate here that including FRAP at different times during microirradiation greatly helps to distinguish between the three models (i.e., excluding models).

In the models presented in this section the FRAP is included by reducing the value of bound PCNA by a factor, which the fit algorithm may adapt for each cell. This accounts for the fact that in these experiments the bleaching of the accumulated PCNA was different, possibly because of a slight shift in the microirradiation/FRAP point, which is because of cell mobility and an offset of the laser focus positions of less than 300 nm.

Fig. 4 shows the microirradiation-FRAP experiments (in addition to the fits of the two kinds of DNA damage model). In the cells 1 to 10 the FRAP bleach was conducted 180 s after the initial DNA damage introducing microirradiation, whereas in the cells 11 to 13 the FRAP bleach was conducted at 1800 s because we wanted to compare the recovery curves from different time points.

Two kinds of DNA damage model

Fig. 4, *A* and *B* show the microirradiation-FRAP experiments and the fitting results of the two kinds of DNA damage model. The curves of cells 11 to 13 were used as validation set and the curves from cells 1 to 10 as training set. The experimental curves can be fitted comparatively well, and the sum of χ^2 over all validation sets is nearly as good as in the fits of the microirradiation data considering that in the microirradiation-FRAP experiments the number of data points is nearly three times as large as in the microirradiation experiments (see Table 1). The parameter values of this validation fit are shown in the fourth row of the microirradiation-FRAP part of Table 1.

As mentioned before, the dissociation rate constant ($k_{SP\rightarrow S+P} \approx 5.2 \times 10^{-3}$) is many orders higher than in the fit of the microirradiation data. Indeed, a FRAP measurement is a good test if dissociation rates are close to zero, because in this case the recovery of the signal after the bleach is exclusively because of the recruitment to sites to which no protein was bound before the bleach. To test whether a dissociation rate constant as low as in the validation fits of the microirradiation data (see $k_{SP\rightarrow S+P}$ in the *upper part* of Table 1) is consistent with the microirradiation-FRAP data we fixed the chemical rate constants on

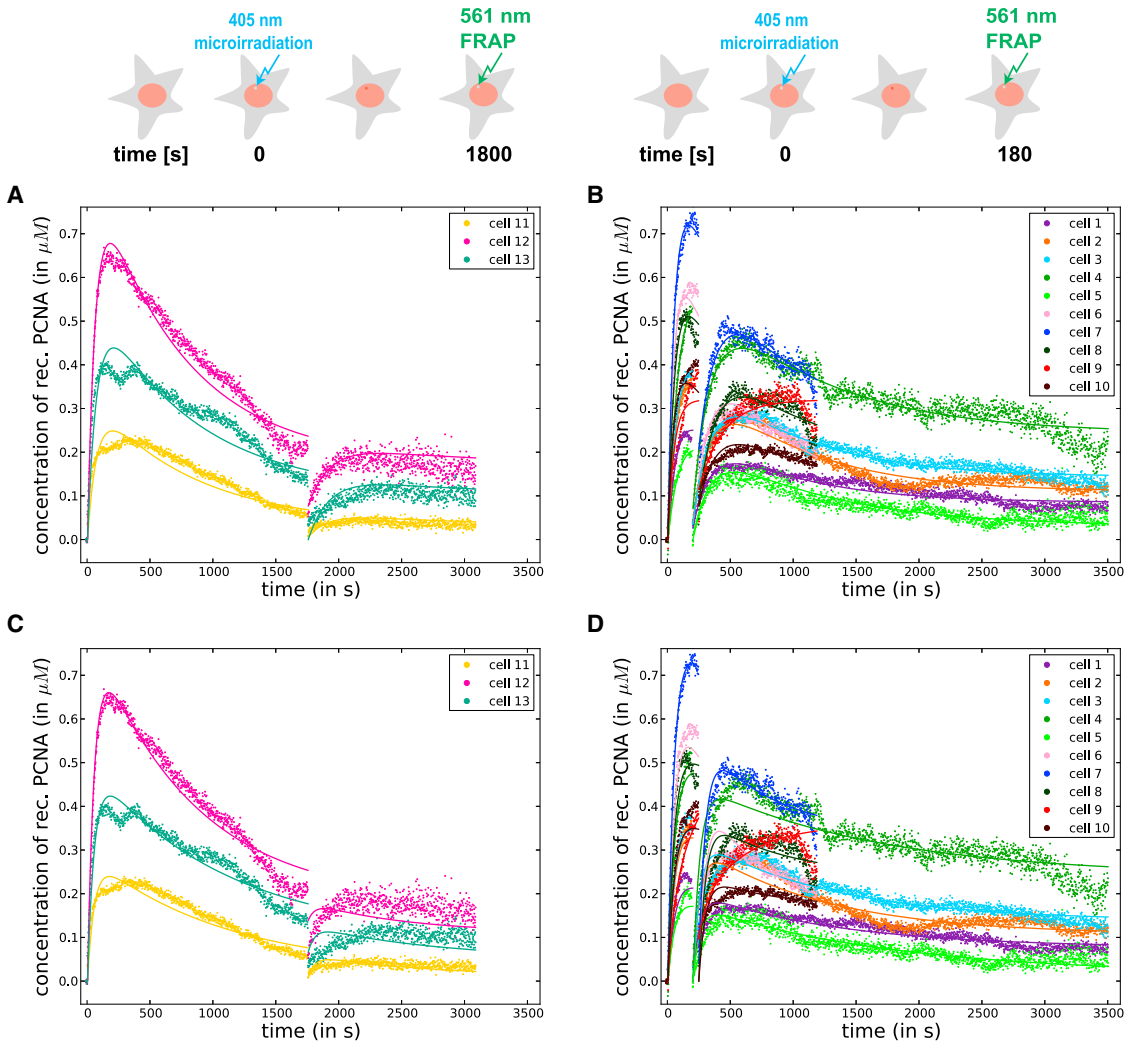

FIGURE 4 Validation (*A*) and training fits (*B*) of the two kinds of DNA damage model to the microirradiation-FRAP data. The experimental data is shown as dots and the fits are shown as lines of the same color. The scheme on top of each plot represents the experimental setup used for the cells whose curves are shown in that plot. The curves from cells 1 to 10 were used as the training set and those from cells 11 to 13 as the validation set. For this model, $\chi^2 \approx 1.2 \times 10^5$. In this validation fit the number of fitted data points was 4650, and the parameter values are shown in the fourth row of the microirradiation-FRAP part of Table 1. (*C* and *D*) Fits of the two kinds of DNA damage model to the microirradiation-FRAP data with the chemical rates being fixed (i.e., they are no free parameters) on the values derived from the fits of this model to the microirradiation data (see the first row of Table 1). All curves were fitted simultaneously. Most importantly, the model fails at fitting the recovery curves from the cells 12 and 13 because of the extremely low dissociation rate constant $k_{SP\to S+P}$, which shows that the chemical rates derived from the microirradiation data are not consistent with the microirradiation-FRAP data. For this model, $\chi^2 \approx 4.4 \times 10^5$ and the number of fitted data points was 16,400. To see this figure in color, go online.

the values derived from the fits of this model to the microirradiation data (*first row* in Table 1) and fitted all the curves from the microirradiation-FRAP data simultaneously. The result is shown in Fig. 4, *C* and *D*. Most importantly, the model fails at fitting the recovery curves from the cells 12 and 13 because of the extremely low dissociation rate constant $k_{SP\to S+P}$. This demonstrates that the results from the fits to the microirradiation data are not reliable because they are not compatible with FRAP experiments conducted after the protein concentration reaches the plateau at around $t = 1800$ s. Contrary to this, the chemical rate constants derived from the fits to the microirradiation-FRAP data are reliable in the sense that they are compatible with the microirradiation data (see Fig. S6).

Influenced-dissociation-rate model

In this section we focus again on the model in which an unknown protein A influences the dissociation rate of PCNA. Fig. 5 *A* shows the validation fits of this model to the microirradiation-FRAP experiments. Again, the curves of cells 11 to 13 were used as the validation set and the curves from cells 1 to 10 as the training set (see Fig. S7). This model fails at fitting the recovery curves from the cells 11 to 13 at $\sim t = 1800$ s and the sum of χ^2 over all four validation sets is 57%

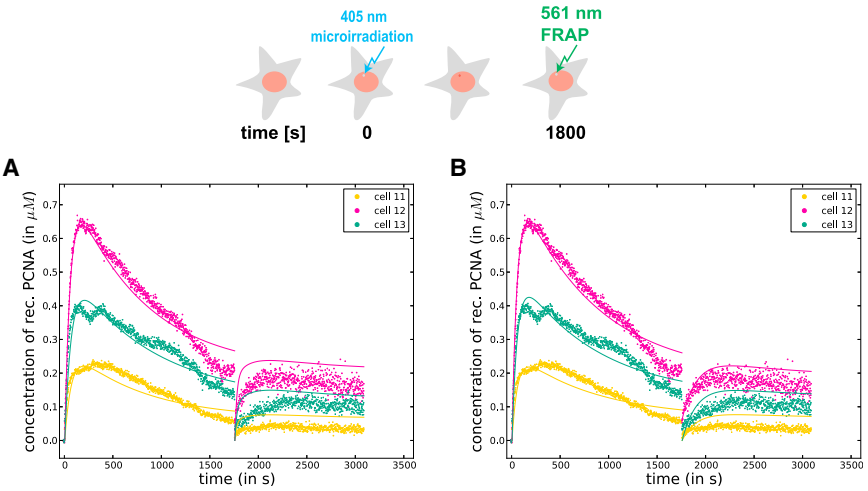

FIGURE 5 (*A*) Validation fits of the influenced dissociation rate model to the microirradiation-FRAP data. For this model, $\chi^2 \approx 2.3 \times 10^5$ and the parameter values are shown in the fourth row of the microirradiation-FRAP part of Table 2. (*B*) Validation fits of the different rates for endogenous proteins model to the microirradiation-FRAP data. For this model, $\chi^2 \approx 1.9 \times 10^5$ and the parameter values are shown in the fourth row of the microirradiation-FRAP part of Table 3. For both models, the curves from cells 1 to 10 were used as the training set (see Fig. S7) and those from cells 11 to 13 as the validation set. The number of fitted data points was 4650. Both models fail at fitting the recovery curves from the cells 11 to 13 around $t = 1800$ s. To see this figure in color, go online.

larger than the sum of χ^2 for the two kinds of DNA damage model (5.5×10^5 against 3.5×10^5). Both are indicators to exclude this model, which was not possible after analyzing the microirradiation data alone (the sum of χ^2 was nearly the same for both models).

Model with different rates for endogenous proteins

The validation fits to the microirradiation-FRAP data of the model in which the endogenous proteins had different rate constants compared with the tagged proteins is shown in Fig. 5 *B*. Again, the curves of cells 11 to 13 were used as the validation set and the curves from cells 1 to 10 as the training set (see Fig. S7). The model fails at fitting the recovery curves from the cells 11 to 13 around $t = 1800s$ similarly to the influenced dissociation rate model. The sum of χ^2 over all four validation sets is much larger than the sum of χ^2 from the other two models (8.7×10^5 against 5.5×10^5 and 3.5×10^5). Hence, these two indicators allow to exclude also this model. This supports the findings of a previous study, in which it was shown that the binding of endogenous and tagged proteins is of equal strength (24).

In summary, the microirradiation-FRAP experiments enabled us to exclude two of three models, which was not possible after analyzing the microirradiation data alone. Additionally, in the sole model not excluded by the microirradiation-FRAP data (the two kinds of DNA damage model) we have shown that the chemical rate constants derived from the fits to the microirradiation data were inconsistent with the microirradiation-FRAP data, whereas the chemical rate constants derived from the microirradiation-FRAP data lead to good fits of the microirradiation data (see Fig. S6).

Table 3 shows a summary of the fitting results of both the microirradiation and the FRAP-microirradiation approach.

DISCUSSION

In the cross-validation fits of the microirradiation data the sum of χ^2 over all four validation fits was $\sum \chi^2 \approx 1.2 \times 10^5$ for the two kinds of DNA damage model as well as the influenced dissociation rate model and

TABLE 3 Parameter values for the different rates for endogenous proteins model

Composition of Validation Set	$k_{S+P\to SP}$ $(\mu M^{-1}s^{-1})$	$k_{S+E\to SE}$ $(\mu M^{-1}s^{-1})$	$k_{SP\to S+P}$ (s^{-1})	$k_{SE\to S+E}$ (s^{-1})	χ^2	No. of Data Points
Microirradiation						
Cells 1–4	1.5×10^{-8}	2.7×10^{-4}	1.9×10^{-2}	2.4×10^{-4}	5×10^4	1980
Cells 5–8	6.8×10^{-9}	3.0×10^{-4}	1.8×10^{-2}	2.6×10^{-4}	4.2×10^4	2340
Cells 9–11	2.6×10^{-9}	3.9×10^{-4}	1.8×10^{-2}	3.2×10^{-4}	3.9×10^4	900
Cells 12–14	3.1×10^{-7}	5.0×10^{-3}	1.5×10^{-3}	3.3×10^{-4}	3.3×10^4	1100
Sum					1.6×10^5	6320
Microirradiation-FRAP						
Cells 1–4	2.8×10^{-2}	7.4×10^{-4}	5.6×10^{-3}	2.5×10^{-5}	3.7×10^5	7000
Cells 5–7	1.9×10^{-2}	6.6×10^{-4}	5.6×10^{-3}	2.1×10^{-4}	1.3×10^5	2950
Cells 8–10	2.5×10^{-2}	9.0×10^{-4}	5.6×10^{-3}	2.4×10^{-4}	1.8×10^5	1800
Cells 11–13	2.2×10^{-2}	6.9×10^{-4}	6.6×10^{-3}	3.2×10^{-4}	1.9×10^5	4650
Sum					8.7×10^5	16,400

The composition of the validation set is given in the column on the left.

$\sum \chi^2 \approx 1.6 \times 10^5$ for the different rates for endogenous proteins model (see Table 4 for a summary of the fitting results). Hence, it was not possible to exclude one of the models based on its ability to fit the data. Contrary to this, in the cross-validation fits of the microirradiation-FRAP data the sum of χ^2 over all four validation fits was $\sum \chi^2 \approx 3.5 \times 10^5$ (two kinds of DNA damage model), $\sum \chi^2 \approx 5.5 \times 10^5$ (influenced dissociation rate model) and $\sum \chi^2 \approx 8.7 \times 10^5$ (model with different rates for endogenous proteins). In addition to this enlarged discrepancy of $\sum \chi^2$, the two latter models obviously failed to fit the recovery curves from all the cells in which the FRAP measurement was conducted at $t = 1800s$ (cells 11 to 13). Based on these findings, it is possible to exclude the influenced dissociation rate model and the model with different rates for endogenous proteins. These results, the exclusion of two out of three models, reveals the usefulness of combining FRAP experiments at different time points after microirradiation: Both, the FRAP recovery curves at the earlier and at later stages, help narrowing down the possible values for the chemical rate constants in such a way that a model might not be able to fit all recovery curves with the same set of chemical rate constants (as in the case of the influenced dissociation rate model and the model with different rates for endogenous proteins).

Additionally, we have shown that the chemical rate constants derived from the fits of the two kinds of DNA damage model to the microirradiation-FRAP data are reliable in the sense that they are compatible with the microirradiation data whereas the fitting results of the same model to the microirradiation data were unreliable, i.e., they are not compatible with the microirradiation-FRAP data.

The biological meaning of our findings is that the overshoot in the experimental data followed by a plateau is possibly attributable to different kinds of DNA damage to which PCNA can bind, such as single- and double-strand breaks, that have distinctly different repair kinetics (32,33,39). From the scenarios we included in our analysis, the two kinds of DNA damage model fitted the data best of the tested models. The fact that the 405 nm laser used in this study to induce damage and subsequent PCNA accumulation is known to induce different types of DNA damage such as pyrimidine dimers, base damage, and DNA double-strand breaks (40) further supports the two kinds of DNA damage model from the biological point of view. Additionally, we could exclude a sole modification of PCNA or a protein influencing it as the reason for this overshoot, given our assumptions are appropriate: relations between chemical species are composed of elementary reactions, recruitment of PCNA and the influencing protein happens on a slower timescale compared with diffusion (see Fig. S1), concentration of freely diffusing PCNA is approximately constant during the period of the experiment.

TABLE 4 Summary of the fitting results of both the microirradiation and the FRAP-microirradiation approach

Model	Two Kinds of DNA Damage	Influenced Dissociation Rate	Different Rates for Endogenous Proteins
Microirradiation			
χ^2	1.2×10^5	1.2×10^5	1.6×10^5
No. of data points	6320	6320	6320
Microirradiation-FRAP			
χ^2	3.5×10^5	5.5×10^5	8.7×10^5
No. of data points	16,400	16,400	16,400

According to our fits of the two kinds of DNA damage model, the dissociation rate constant of PCNA $k_{SP \to S+P}$ is in between $4.3 \times 10^{-3} s^{-1}$ and $6.2 \times 10^{-3} s^{-1}$, which is in agreement with a previous analysis of nucleotide excision repair in which k_{off} for PCNA was reported to be in between $2 \times 10^{-3} s^{-1}$ and $5 \times 10^{-2} s^{-1}$ depending on the status of the DNA (36). The association constant, which lies between $2.8 \times 10^{-3} \mu M^{-1} s^{-1}$ and $3.5 \times 10^{-3} \mu M^{-1} s^{-1}$ in our model, is also consistent with previous models (ranging from $1.0 \times 10^{-3} \mu M^{-1} s^{-1}$ to $0.31 \times 10^{-1} \mu M^{-1} s^{-1}$ (36)).

In the influenced dissociation rate model we assumed that an unknown protein binds to the same substrate (damaged DNA) as PCNA thereby increasing the dissociation rate of PCNA. An alternative but ultimately similar situation would be present if before the recruitment of PCNA protein A was already bound to all substrates. Contrary to the influenced dissociation rate model, in this alternative situation the dissociation of A would take place after the recruitment of PCNA thereby increasing the dissociation rate of PCNA. Such a process could be modeled by essentially the same differential equations as in the influenced dissociation rate model. Hence, this alternative reason for the overshoot shown in our experimental data is also excluded by the FRAP-microirradiation data.

It has been reported that the binding of tagged and untagged endogenous proteins is of equal strength (24). With the microirradiation-FRAP approach presented in this article, we have shown indeed that the model that uses a different binding strength for tagged and endogenous proteins is not consistent with the microirradiation-FRAP experiments. Even though this information was available before, including this model into our analysis demonstrated the usefulness of this approach regarding the exclusion of alternative models.

We have shown that it is feasible to conduct FRAP experiments during the early recruitment phase, which to our knowledge has not been done before. This is especially important if the observed processes are so slow that they do not reach an equilibrium during the time of the experiment. We have also presented a theoretical approach to analyze such microirradiation-FRAP experiments that does not rely on the equilibrium condition that is a rather limiting condition of classical FRAP analysis (5,7–9).

FRAP experiments during the recruitment phase are of great importance if the chemical rate constants change during the recruitment phase. Some of the possible reasons are posttranslational modifications of a protein and the assembling of multiprotein complexes in which the involved proteins influence each other. In a previous study, we presented a detailed theoretical analysis of different models describing such situations (22).

In general, FRAP experiments are particularly sensitive to the dissociation rate constant, whereas recruitment curves strongly depend on the association rate constant. Microirradiation-FRAP experiments similar to those presented in this article give special insight because they are sensitive to both the association rate and the dissociation rate constant. This is due to the recruitment still happening while the recovery from the FRAP bleach takes place. Because of this combination of recruitment and recovery, the analysis of microirradiation-FRAP data can be more complicated compared with microirradiation and FRAP data alone, but this is rewarded by the ability to compare the chemical rate constants at different time points, which allows deriving more reliable values for the chemical rate constants and excluding alternative models.

In this study we used models as simple as possible because with increasing complexity any model will fit almost every data set well, which makes it impossible to discriminate between different models based on their ability to reproduce the data. Of course, more complicated models would probably reduce the χ^2 value for the cross-validation fits even further, but the higher number of free parameters would lead to a greater space of possible solutions and one may thus not be able to conclude which are the most important (or the minimum set of) interactions causing the experimental observations. Nevertheless, our theoretical approach used to analyze the microirradiation-FRAP data is easily adapted to more complex models. For example, if diffusion happens on a similar timescale as recruitment our approach may be combined with a diffusion model (41,42). Actually, with increasing model complexity the information from the microirradiation-FRAP data will be even more valuable.

Additionally, our approach may be used to study less complex situations, for example, when using other lasers than those from the experiments shown here to avoid specific types of damage (43). If it is possible to induce only one specific type of damage, the microirradiation-FRAP approach could be especially useful to derive reliable values for the rate constants and to analyze whether or not the chemical rate constants of the involved proteins change during the recruitment.

SUPPORTING MATERIAL

Supporting Materials and Methods, seven figures, and one table are available at http://www.biophysj.org/biophysj/supplemental/S0006-3495(15)00866-8.

AUTHOR CONTRIBUTIONS

M.C.C. designed research and wrote the article; B.D. designed research and wrote the article; L.L. designed research, performed research, contributed analytic tools, analyzed data, and wrote the article; N.L. contributed analytic tools and wrote the article; B.M. performed research; D.N. performed research; and A.R. designed research, wrote the article, and contributed analytic tools.

ACKNOWLEDGMENTS

This work was supported by the German Research Council (DFG GRK 1657, Project 1B, 1C, and 3A). Additionally, this work was supported in part by a grant of the Federal Ministry of Education and Research (BMBF 02NUK017D) to M.C.C and also in part to A.R. (BMBF 02NUK036D).

REFERENCES

1. Klein, C., and F. Waharte. 2010. Analysis of molecular mobility by fluorescence recovery after photobleaching in living cells. *In* Microscopy: Science, Technology, Applications and Education. Formatex Research Center, Badajoz, Spain, pp. 772–783.
2. Cole, N. B., C. L. Smith, …, J. Lippincott-Schwartz. 1996. Diffusional mobility of Golgi proteins in membranes of living cells. *Science.* 273:797–801.
3. Misteli, T. 2001. Protein dynamics: implications for nuclear architecture and gene expression. *Science.* 291:843–847.
4. Reits, E. A., and J. J. Neefjes. 2001. From fixed to FRAP: measuring protein mobility and activity in living cells. *Nat. Cell Biol.* 3:E145–E147.
5. Carrero, G., D. McDonald, …, M. J. Hendzel. 2003. Using FRAP and mathematical modeling to determine the in vivo kinetics of nuclear proteins. *Methods.* 29:14–28.
6. Mueller, F., D. Mazza, …, J. G. McNally. 2010. FRAP and kinetic modeling in the analysis of nuclear protein dynamics: what do we really know? *Curr. Opin. Cell Biol.* 22:403–411.
7. Phair, R. D., P. Scaffidi, …, T. Misteli. 2004. Global nature of dynamic protein-chromatin interactions in vivo: three-dimensional genome scanning and dynamic interaction networks of chromatin proteins. *Mol. Cell. Biol.* 24:6393–6402.
8. Sprague, B. L., and J. G. McNally. 2005. FRAP analysis of binding: proper and fitting. *Trends Cell Biol.* 15:84–91.
9. Rabut, G., V. Doye, and J. Ellenberg. 2004. Mapping the dynamic organization of the nuclear pore complex inside single living cells. *Nat. Cell Biol.* 6:1114–1121.
10. Mortusewicz, O., H. Leonhardt, and M. C. Cardoso. 2008. Spatiotemporal dynamics of regulatory protein recruitment at DNA damage sites. *J. Cell. Biochem.* 104:1562–1569.
11. Mailand, N., I. Gibbs-Seymour, and S. Bekker-Jensen. 2013. Regulation of PCNA-protein interactions for genome stability. *Nat. Rev. Mol. Cell Biol.* 14:269–282.
12. Hedglin, M., R. Kumar, and S. J. Benkovic. 2013. Replication clamps and clamp loaders. *Cold Spring Harb. Perspect. Biol.* 5:a010165.
13. Görisch, S., and M. Cardoso. 2006. PCNA and DNA replication (I). *In* Proliferating Cell Nuclear Antigen. H. Lee and M. Szyf, editors. Research SignPost, Kerala, India, pp. 51–70.
14. Ulrich, H. D., and T. Takahashi. 2013. Readers of PCNA modifications. *Chromosoma.* 122:259–274.
15. Palle, K., and C. Vaziri. 2011. Rad18 E3 ubiquitin ligase activity mediates Fanconi anemia pathway activation and cell survival following DNA topoisomerase 1 inhibition. *Cell Cycle.* 10:1625–1638.

16. Hoege, C., B. Pfander, …, S. Jentsch. 2002. RAD6-dependent DNA repair is linked to modification of PCNA by ubiquitin and SUMO. *Nature.* 419:135–141.

17. Herce, H. D., M. Rajan, …, M. C. Cardoso. 2014. A novel cell permeable DNA replication and repair marker. *Nucleus.* 5:590–600.

18. Ciccia, A., A. V. Nimonkar, …, S. J. Elledge. 2012. Polyubiquitinated PCNA recruits the ZRANB3 translocase to maintain genomic integrity after replication stress. *Mol. Cell.* 47:396–409.

19. Bruning, J. B., and Y. Shamoo. 2004. Structural and thermodynamic analysis of human PCNA with peptides derived from DNA polymerase-δ p66 subunit and flap endonuclease-1. *Structure.* 12:2209–2219.

20. Zhu, Q., Y. Chang, …, Q. Wei. 2014. Post-translational modifications of proliferating cell nuclear antigen: a key signal integrator for DNA damage response (review). *Oncol. Lett.* 7:1363–1369.

21. Harper, J. W., and S. J. Elledge. 2007. The DNA damage response: ten years after. *Mol. Cell.* 28:739–745.

22. Lengert, L., and B. Drossel. 2013. Deducing underlying mechanisms from protein recruitment data. *PLoS One.* 8:e66590.

23. Landry, J. J., P. T. Pyl, …, L. M. Steinmetz. 2013. The genomic and transcriptomic landscape of a HeLa cell line. *G3 (Bethesda).* 3:1213–1224.

24. Sporbert, A., P. Domaing, …, M. C. Cardoso. 2005. PCNA acts as a stationary loading platform for transiently interacting Okazaki fragment maturation proteins. *Nucleic Acids Res.* 33:3521–3528.

25. Rottach, A., E. Kremmer, …, U. Rothbauer. 2008. Generation and characterization of a rat monoclonal antibody specific for PCNA. *Hybridoma (Larchmt).* 27:91–98.

26. Lan, L., S. Nakajima, …, A. Yasui. 2005. Accumulation of Werner protein at DNA double-strand breaks in human cells. *J. Cell Sci.* 118:4153–4162.

27. Schneider, C. A., W. S. Rasband, and K. W. Eliceiri. 2012. NIH Image to ImageJ: 25 years of image analysis. *Nat. Methods.* 9:671–675.

28. Sprague, B. L., R. L. Pego, …, J. G. McNally. 2004. Analysis of binding reactions by fluorescence recovery after photobleaching. *Biophys. J.* 86:3473–3495.

29. Morris, G. F., and M. B. Mathews. 1989. Regulation of proliferating cell nuclear antigen during the cell cycle. *J. Biol. Chem.* 264:13856–13864.

30. Lele, T. P., and D. E. Ingber. 2006. A mathematical model to determine molecular kinetic rate constants under non-steady state conditions using fluorescence recovery after photobleaching (FRAP). *Biophys. Chem.* 120:32–35.

31. Kong, X., S. K. Mohanty, …, M. W. Berns. 2009. Comparative analysis of different laser systems to study cellular responses to DNA damage in mammalian cells. *Nucleic Acids Res.* 37, e68–e68.

32. Choi, J.-H., S. Gaddameedhi, …, A. Sancar. 2014. Highly specific and sensitive method for measuring nucleotide excision repair kinetics of ultraviolet photoproducts in human cells. *Nucleic Acids Res.* 42:e29.

33. Schermerhorn, K. M., and S. Delaney. 2014. A chemical and kinetic perspective on base excision repair of DNA. *Acc. Chem. Res.* 47:1238–1246.

34. Solomon, D. A., M. C. Cardoso, and E. S. Knudsen. 2004. Dynamic targeting of the replication machinery to sites of DNA damage. *J. Cell Biol.* 166:455–463.

35. Hansen, N. 2006. The CMA evolution strategy: a comparing review. *In* Towards a New Evolutionary Computation. Advances on Estimation of Distribution Algorithms. J. Lozano, P. Larranaga, I. Inza, and E. Bengoetxea, editors. Springer, Heidelberg, Germany, pp. 75–102.

36. Luijsterburg, M. S., G. von Bornstaedt, …, T. Höfer. 2010. Stochastic and reversible assembly of a multiprotein DNA repair complex ensures accurate target site recognition and efficient repair. *J. Cell Biol.* 189:445–463.

37. Cazzalini, O., S. Sommatis, …, E. Prosperi. 2014. CBP and p300 acetylate PCNA to link its degradation with nucleotide excision repair synthesis. *Nucleic Acids Res.* 42:8433–8448.

38. Görisch, S. M., A. Sporbert, …, M. C. Cardoso. 2008. Uncoupling the replication machinery: replication fork progression in the absence of processive DNA synthesis. *Cell Cycle.* 7:1983–1990.

39. Hirayama, R., Y. Furusawa, …, K. Ando. 2005. Repair kinetics of DNA-DSB induced by x-rays or carbon ions under oxic and hypoxic conditions. *J. Radiat. Res. (Tokyo).* 46:325–332.

40. Dinant, C., M. de Jager, …, W. Vermeulen. 2007. Activation of multiple DNA repair pathways by sub-nuclear damage induction methods. *J. Cell Sci.* 120:2731–2740.

41. Crank, J. 1975. The Mathematics of Diffusion. Clarendon Press, Oxford, UK.

42. Soumpasis, D. M. 1983. Theoretical analysis of fluorescence photobleaching recovery experiments. *Biophys. J.* 41:95–97.

43. Träutlein, D., M. Deibler, …, E. Ferrando-May. 2010. Specific local induction of DNA strand breaks by infrared multi-photon absorption. *Nucleic Acids Res.* 38:e14.

Discrimination of Kinetic Models by a Combination of Microirradiation and Fluorescence Photobleaching

Laurin Lengert,[1*] Nicor Lengert,[1] Barbara Drossel,[1] M. Cristina Cardoso,[2] Britta Muster,[2] Danny Nowak,[2] Alexander Rapp[2]

1 Institute for Condensed Matter Physics, Technische Universität Darmstadt, 64289 Darmstadt, Germany
2 Department of Biology, Technische Universität Darmstadt, 64287 Darmstadt, Germany
*To whom correspondence should be addressed; E-mail: lengert@fkp.tu-darmstadt.de.

Supporting Material

Control experiments

We performed several control experiments in order to address the following questions, all of which give important insights into the experimental conditions and hence have to be considered in our theoretical modeling:

1. Does the 561 nm laser induce damage to which PCNA is recruited?
2. Is diffusion relevant on the timescale of the fluorescence recovery after microirradiation?
3. Is the bleaching of the proteins reversible?
4. Does the total amount of PCNA change during the time span of our experiments?
5. Does the concentration of freely diffusing PCNA change during our experiments?

In the first part of the control experiments we addressed the first two questions. To test whether or not the 561 nm laser induces damage to which PCNA is recruited we measured the fluorescence signal in the bleachspot after irradiating four cell nuclei for 0.8 seconds with the 561 nm laser set to 100% resulting in 5.4 mJoule. The data analysis was done in the same way as for the recruitment experiments (see method section). Hence, the resulting curves represent the concentration of recruited proteins within the bleachspot. If the 561 nm laser had introduced DNA damage to which PCNA had been recruited, the concentration of recruited PCNA would have increased above zero. This is not the case as can be seen in figure S1A. At $t = 0$ the concentration drops below zero due to the bleach reducing the signal intensity in the bleachspot below the average fluorescence signal (based on the total nucleus area), due to photobleaching. Shortly after the bleach the concentrations (intensities) recover to the pre-bleach value, zero. This recovery is due to the diffusion of the proteins and happens on a much faster time scale (about 4 seconds, see supplementary figures S1A and S1D) compared to the recruitment process (a few hundred seconds, see result section). Also, we followed the conclusions from Sprague et al. (1) by showing that the recovery curves are independent of the bleach spot size (supplementary figure S1C-E). This justifies not to include diffusion in our theoretical models.

During the first eight minutes the curves do not significantly rise above zero. Hence, we can conclude that the 561 nm laser does not induce damage to which PCNA is recruited. For some of the cells the curves end earlier than for others. The reason is that in those experiments the cells moved too far from their initial position, which made the image analysis after that time point unreliable (this is also the reason for the truncated datasets shown in all other figures).

In the second part of the control experiments we addressed the third and fourth question: Is the bleaching of the proteins reversible and does the total amount of PCNA change during the time span of our experiments? To answer this we used the same experimental data as in the previous control, but instead of the concentration of bound proteins in the bleachspot, we analyzed the nucleus fluorescence signal (NFS(t)), which is shown in figure S1B. At the beginning the signal drops due to the bleaching. In the first minute in some cells the signal slightly decreases due to the additional bleaching caused by the constant imaging. After the first minute the signal in all curves changes only insignificantly (the relative slope of the linear fits is nearly zero, see table S1). This leads to the conclusion that the total amount of PCNA does not change during our experiments and that the bleaching of the proteins is irreversible. This is also supported by the findings in a previous paper (2). Both are important informations needed for theoretical modeling.

To address the fifth question we analyzed the same images from FRAP experiments which we will use in the result section. But, instead of the signal from the bleachspot, we analyzed the signal from a region of the cell nucleus that was neither microirradiated nor photobleached (except the inevitable bleaching from imaging). The signal of this non bleached region is denoted by SNBR(t), the size of this region is denoted by $\text{SNBR}_{\text{Area}}$ and its depth in z direction by w_z. With this, to derive the concentration of free PCNA proteins within this non bleached region ($\text{PCNA}_{\text{free}}$) we used a variation of eq. 3:

$$\text{PCNA}_{\text{free}}(\text{t}) = \frac{v}{\text{SNBR}_{\text{Area}} w_z} \frac{1}{\text{BF(t)}} \left(\text{SNBR(t)} - \text{BGS(t)} \frac{\text{SNBR}_{\text{Area}}}{\text{BGS}_{\text{Area}}} \right) \tag{1}$$

In figure S4 $\text{PCNA}_{\text{free}}$(t) is shown for the thirteen cells, which we will use in the result section. It is important to notice that most of the time this concentration does not change significantly. Hence, the concentration of free proteins is approximately constant during the period of the experiment. This validates an important assumption made in our theoretical models. Only shortly after microirradiation and after the FRAP bleach do the curves change significantly which is due to the diffusion of the proteins.

Table S1: Slope and relative slope for the linear fits shown in figure S1B.

cell	slope m (in a.u. s^{-1})	relative slope $\frac{m}{f(t=70s)}$ (in s^{-1})
1	-187	-6.5×10^{-5}
2	-354	-1.8×10^{-4}
3	-19	-3.2×10^{-6}
4	-345	-6.6×10^{-5}

Supporting References

[1] Sprague, B. L., R. L. Pego, D. A. Stavreva, and J. G. McNally. 2004. Analysis of binding reactions by fluorescence recovery after photobleaching. *Biophysical journal*, 86(6):3473–3495.

[2] Sporbert, A., A. Gahl, R. Ankerhold, H. Leonhardt, and M. Cardoso. 2002. DNA polymerase clamp shows little turnover at established replication sites but sequential de novo assembly at adjacent origin clusters. *Molecular Cell*, 10:1355–1365.

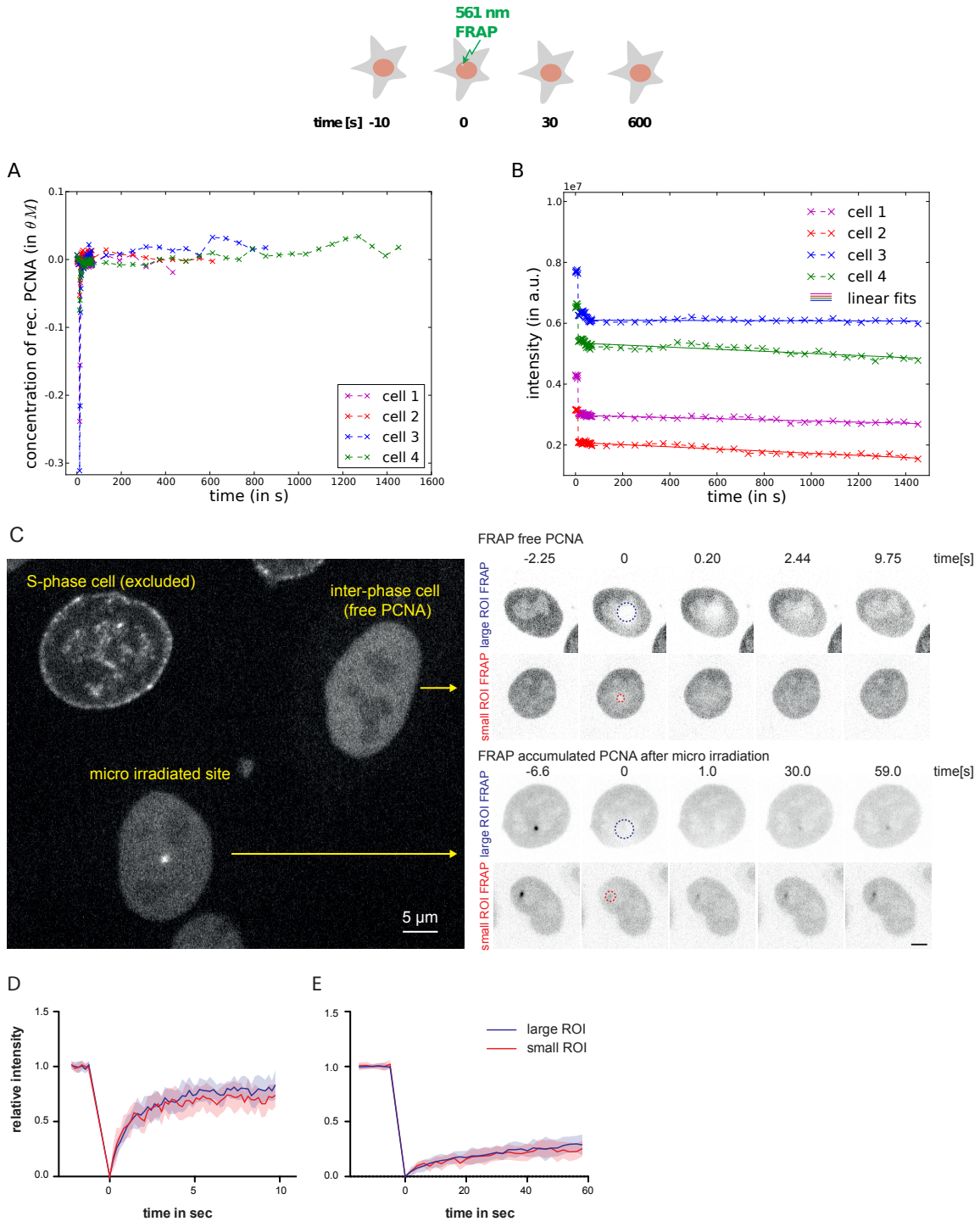

Figure S1: A) Concentration of recruited proteins after a FRAP bleach (561 nm laser). B) Corresponding nucleus fluorescence signal (NFS). The data after $t = 70$ s was fitted by a linear fit $f(t) = mt + a$ minimizing least squares. The resulting slopes are shown in table S1. Experimental setup according to scheme on top. C) HeLa cells stabily expressing mCherry-PCNA were analyzed by FRAP. Only non S-phase cells were selected and the mobility of either free PCNA (C, upper right) or PCNA accumulated at sites of microirradiation (C, lower right) were analyzed with different sizes of FRAP-ROI. Analysis of more than 15 cells per condition shows independence of the FRAP parameters from the ROI size for both free PCNA (D) and PCNA accumulated at sites of microirradiation (E). Also the different time scales become visible during which recovery occurs in the unbound and accumulated PCNA populations.

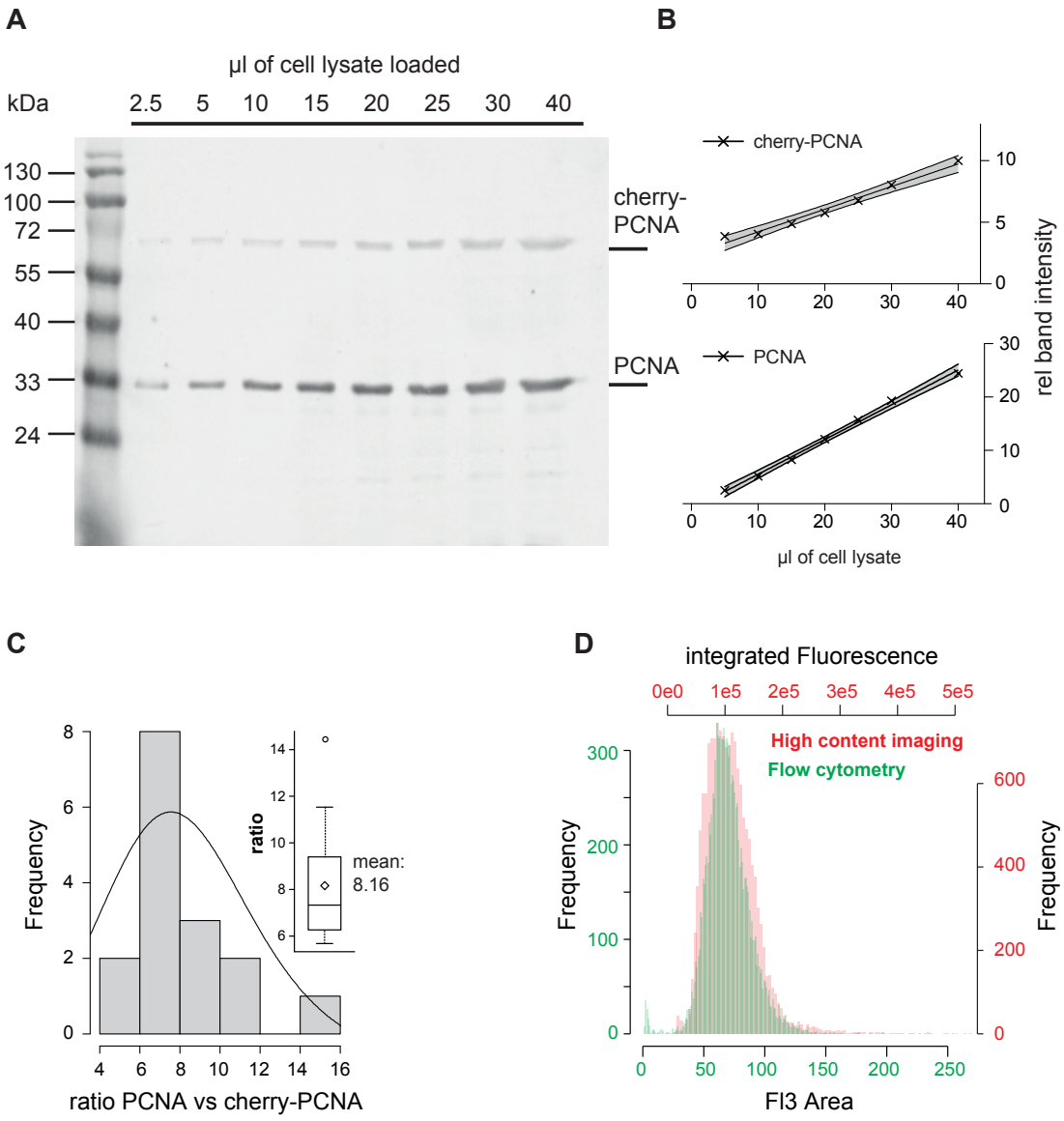

Figure S2: Determination of the level of endogenous versus fluorescently tagged PCNA. A) Quantitative western blot depicting the simultaneous detection of endogenous PCNA as well as stably transfected mCherry-PCNA. Increasing amounts of cell lysate were loaded. To select bands within the linear detection limit the intensity vs amount plots were generated (B) and only values within the 95% confidence interval were used for calculation of the ratios. C) Histogram of the ratios of PCNA vs mCherry-PCNA. The inset shows the distribution as a boxplot. The ratio obtained from 3 blots and 16 band-pairs meeting the quality criteria (B) was 8.1 ± 2.7 (mean± SD). D) Total nuclear intensity distribution of HeLa Kyoto mCherry-PCNA cells used in the study as measured by flow cytometry and high content imaging. The cells showed a variation in fluorescence intensity within the reported 2 fold variation of endogenous PCNA during the cell cycle (Flow cytometry: n=11,972; mean: 70; STD: 19; Coefficient of variation: 26.8; high content imaging: n=14,932; mean: 109,514; STD: 44,443; Coefficient of variation: 40.6)

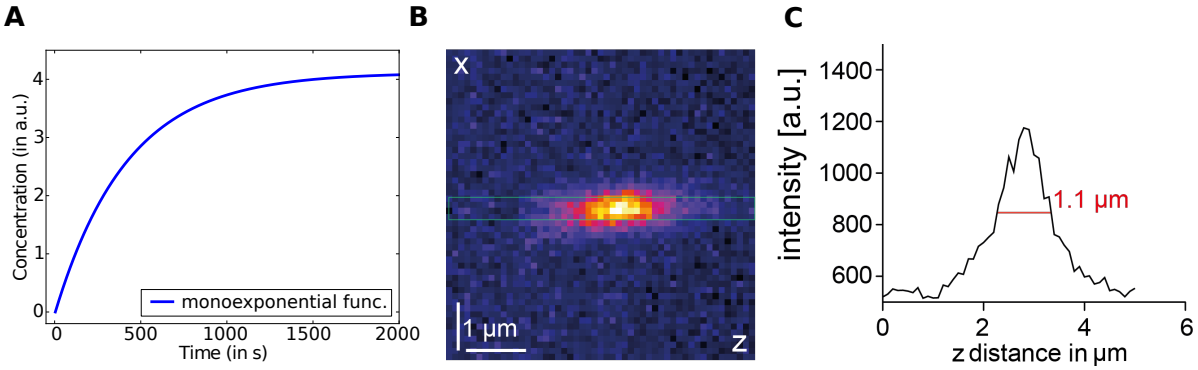

Figure S3: A) Plotted is an exemplary monoexponential function. Those functions are the solutions of our basic model, which includes only two chemical species, the PCNA protein and sites of DNA damage, as well as one chemical reaction for the binding of PCNA and one for its dissociation (eq. R1 and R2). B) Recorded point spread function obtained from fluorescent 100 nm beads (TetraSpeck Microspheres, 0.1 µm, Life Technologies), with imaging settings identical to the ones used in the experiments. XZ-projection was obtained from Volocity (Perkin Elmer). C) Measurement of the point spread function in z direction as indicated in B) by the green square. The full width half maximum was measured after background substraction.

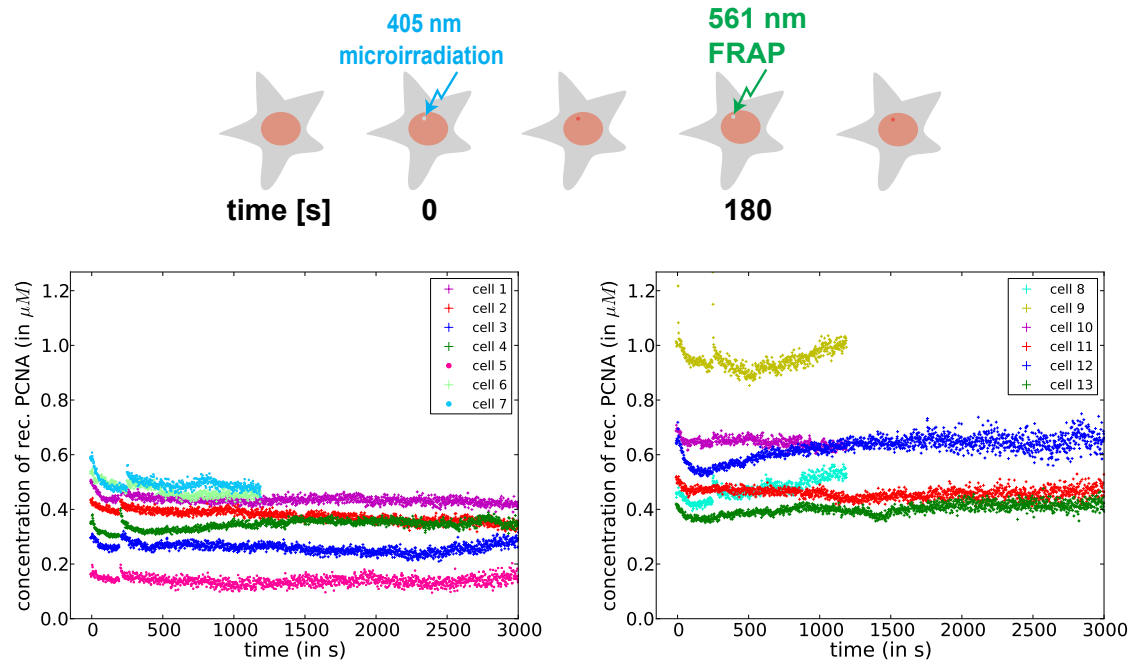

Figure S4: Control experiments that show the concentration of PCNA proteins in a region that was not bleached. Experimental setup according to scheme on top. The thirteen curves were split into two groups for better distinguishability. The different concentration levels between the curves are possibly due to the cells differing in cell size and the amount of tagged proteins and are of no further importance. Whereas, for the assumptions made in our theoretical models it is important that the curves are rather constant except shortly after the microirradiation and the FRAP bleach.

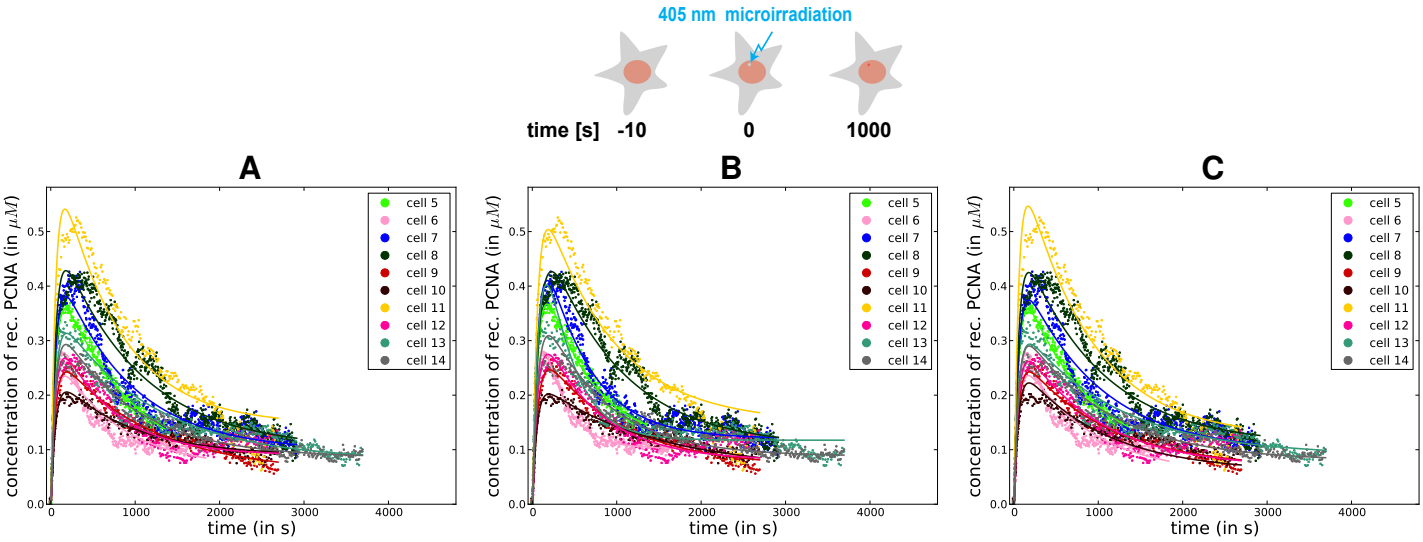

Figure S5: A) Training fits of the "two kinds of DNA damage" model to the microirradiation data. Parameter values are shown in the first row of table 1. B) Training fits of the model in which the dissociation rate of PCNA is influenced by a hypothetical protein denoted by A. Parameter values are shown in the first row of table 2. C) Training fits of the "different rates for endogenous proteins" model. Parameter values are shown in the first row of table 3. The experimental data is shown as dots and the fits are shown as lines of the same color. Experimental setup according to scheme on top.

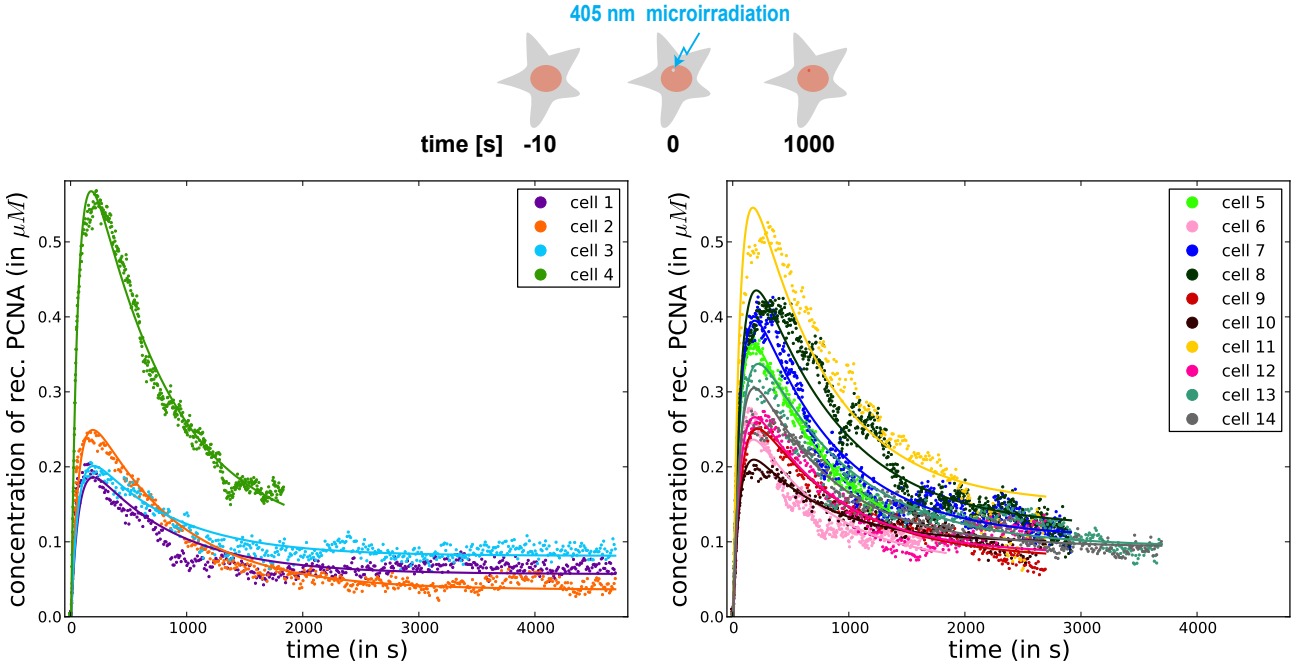

Figure S6: Fit of the "two kinds of DNA damage" model to the microirradiation data with the chemical rates being fixed (i.e. they are no free parameters) on the values derived from the fits of this model to the microirradiation-FRAP data (values shown in fourth row of the microirradiation-FRAP part of table 1). All curves were fitted simultaneously. The experimental data is shown as dots and the fits are shown as lines of the same color. The scheme on top of each plot represents the experimental setup used for the cells whose curves are shown in that plot. $\chi^2 \approx 1.1 \times 10^5$ and the number of fitted datapoints was 6,320. This fit shows that the chemical rates derived from the microirradiation-FRAP experiments are consistent with the microirradiation data.

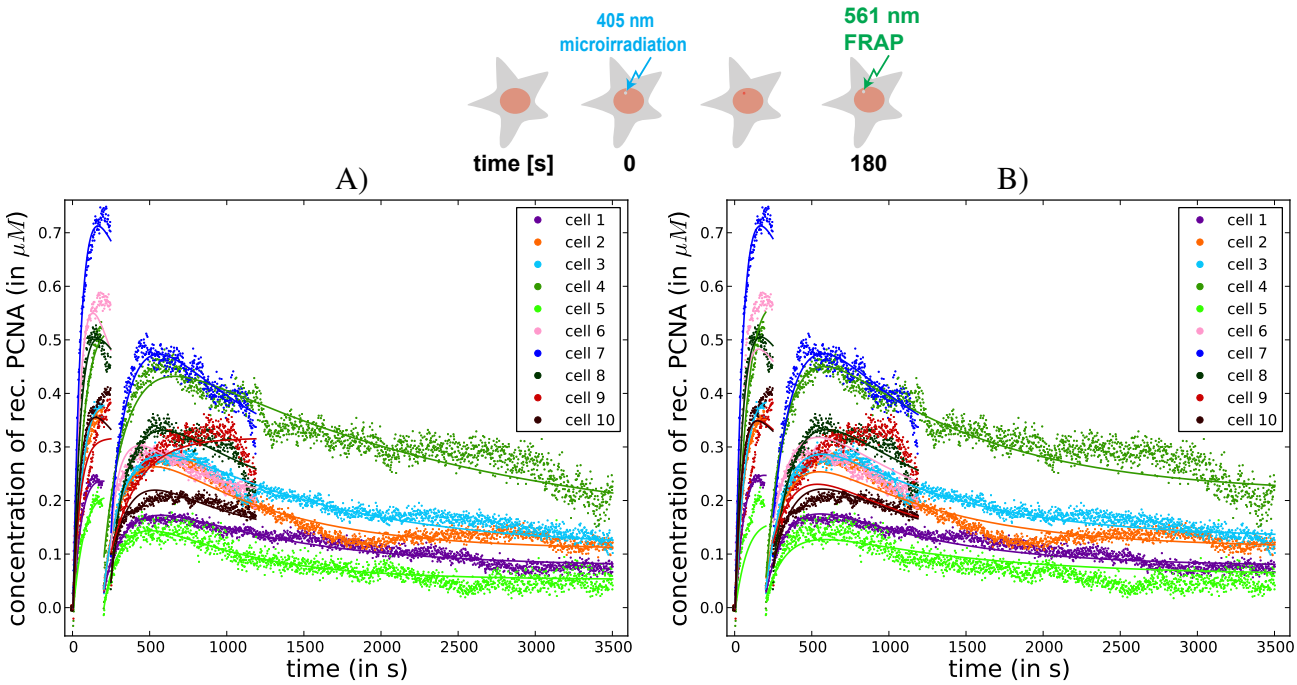

Figure S7: A) Training fits of the "influenced dissociation rate" model to the microirradiation-FRAP data. The resulting parameter values are shown in the fourth row of the microirradiation-FRAP part of table 2. B) Training fits of the "different rates for endogenous proteins" model to the microirradiation-FRAP data. The resulting parameter values are shown in the fourth row of the microirradiation-FRAP part of table 3. The experimental data is shown as dots and the fits are shown as lines of the same color. Experimental setup according to scheme on top.